LA-UR-19-28813

Title: Evaluating Corrosion Effects on the Stainless Steel Components of the SAVY-4000/Hagan Nuclear Material Storage Containers: FY19 Update

Author(s): Narlesky, Joshua Edward; Davis, John Taylor; Dumont, Joseph Henry; Duque, Juan G.; Karns, Tristan; Kaufeld, Kimberly Ann; Kelly, Elizabeth J.; Oka, Jude M.; Rios, Daniel; Smith, Paul Herrick; Stone, Timothy Amos; Vaidya, Rajendra U.; Wendelberger, James G.

Intended for: Report

Issued: 2019-10-11 (rev.1)

Evaluating Corrosion Effects on the Stainless Steel Components of the SAVY-4000/Hagan Nuclear Material Storage Containers: FY19 Update

Authors:

Joshua Narlesky
John Davis
Joseph Dumont
Juan Duque
Tristan Karns
Kimberly Kaufeld
Elizabeth Kelly
Jude Oka
Daniel Rios
Paul Smith
Timothy Stone
Rajendra Vaidya
Jim Wendelberger

Rev. 1, October 8, 2019

Table of Contents

1.0 Introduction

This report provides an update of the FY19 corrosion observations, laboratory studies, and mitigation efforts for the nuclear material storage program at Los Alamos National Laboratory. Nuclear material packages outside of an approved engineered contamination barrier must meet packaging, surveillance, and testing requirements designed to protect workers from airborne contamination per Department of Energy (DOE) Manual 441.1-1, *Nuclear Material Packaging.*[1] The SAVY-4000 containers were developed at Los Alamos National Laboratory (LANL) in conjunction with Nuclear Filter Technology as a manually-compliant container system for staging and storage of plutonium for LANL and the DOE complex. The SAVY-4000 containers have a 316L stainless steel containment barrier, which was selected based on its corrosion resistance properties. These containers were approved for use in 2014 with a five-year design life. LANL has requested and DOE has approved lifetime extension from 5 to 15 years. The 10-year lifetime extension was proposed as a conservative recommendation based on the corrosion observations for the metal components in surveillance and laboratory studies.[2]

A surveillance program for SAVY-4000 containers was established per DOE M 441.1-1 requirements to ensure that they continue to meet their design criteria. The surveillance program evaluates the aging of the container components during the storage lifetime. Surveillance includes a visual inspection with the objective of identifying early indications of package degradation. The visual inspection has found corrosion each year since FY15 in storage containers. Concern that corrosion could affect the design life of the container components led to the formation of a corrosion working group tasked with determining the conditions that support corrosion of the stainless steel components and the impact of that corrosion on the containers. The corrosion working group (CWG) has been investigating several aspects of corrosion of the stainless steel components of the SAVY-4000 and Hagan storage containers including the following:

- Targeted surveillance of the most aggressive storage conditions
- Corrosive gases: sources and mitigation
- Wall thinning due to general corrosion
- Susceptibility of storage containers to through-wall penetration due to pitting
- Susceptibility of storage containers to through-wall penetration due to stress corrosion cracking.

Selection of containers for surveillance is documented in the field surveillance plan.[3] Container selection relies on engineering judgement to identify packages exposed to the most aggressive storage conditions with respect to radiation dose and potentially corrosive contents. The FY19 surveillance plan targeted SAVY-4000 and Hagan containers with similar/same IDC type as containers that showed corrosion in the past as well as the previously identified "worst-case IDC groups" not yet examined. For storage containers that fall within the same IDC grouping, preference was given to containers higher in age, higher in wattage, higher in nuclear material content, and smaller in size. These factors have been found to correlate with the degradation of PVC bags, resulting in higher rates of HCl generation.[4] Additionally, engineering judgment targeted material types that would result in higher alpha and/or gamma dose as well as a higher thermal load to the PVC bag. These conditions include continuing examination of Pu-238 (MT-83) containers; the addition of material types not previously examined include MT-82 (Np-237, which has a high gamma dose), and MT-41 and MT-42 (Pu-242, which is high in Am-241); and large MT-56 and MT-57 (> 20% Pu-240, which are also high in Am-241).[3] The results of this years' visual examination and trending analyses are discussed in Section 2.1.

Past work has identified the primary source of the corrosive gases is the dehydrochlorination of PVC. Gamma irradiation of PVC causes degradation of the polymer backbone (double-bond formation, polymer cross-linking and chain scission).[5] This results in PVC discoloration, brittleness and loss of strength as well as production of HCl gas. Alpha irradiation also causes dehydrochlorination of PVC, especially in combination with high temperature. Production of HCl gas increases with increasing beta/gamma dose. This is consistent with observations of highly degraded bags in packages high in Am-241. A second potential source of HCl (and Cl_2) is the radiolysis of hydrated salt compounds when these compounds are present in the material matrix.[6] However, previous experiments with MSE salt materials have shown that the corrosive gas generation requires significant moisture adsorption (in excess of 0.5 wt%), which would be mitigated by the dry atmosphere of the PF4 glovebox line, the bag out bag surrounding the inner container and sealed with tape, and thermal gradients due to the radioactive decay heat that drive moisture out of the container.[7] As a result, the focus of current efforts in this area is the replacement of the PVC bag with a material, such as aromatic polyurethane (APU) that does not produce corrosive gases. The replacement material for the PVC is discussed in Section 5.0.

Wall thinning was previously identified as a potential failure mechanism of SAVY-4000 and Hagan containers based on the extent of the general corrosion observed in FY16 on transfer containers 20T and 21T (referred to in this report as the SAI Containers) that were packaged with solutions of Pu dissolved in 3M HCl.[8] These containers were previously examined and no significant change in wall thickness was observed. The instrumentation used to examine these containers is undergoing design and testing for installation in PF4 for wall thickness measurements as well as nondestructive identification of defects (pits and cracks) in the container wall.[8] Development of this equipment is discussed in Section 6.4.

Pitting was identified as a potential failure mechanism based on the results of surveillance container 16H1 (referred to in this report as XBPS333). This container was selected for surveillance based on the observation of a white powder deposited on the outside of the filter and on the surrounding storage compartment surfaces[9]. Optical microscopy found pitting on the lid (5 to 15 microns in diameter) and sidewall (100-160 microns in diameter). Depths were estimated to be approximately 20 to 40 microns. Assuming a maximum depth of 40 microns, the maximum penetration of the sidewall was approximately 5% after 8 years. A conservative pit growth model shows that the pit would not breach the sidewall in a 40-year lifetime.

The greatest concern with respect to the corrosion of currently packaged SAVY-4000 and Hagan containers is through-wall cracking resulting from SCC of stainless steel. Based on the recommendations of the corrosion working group, a series of tests were performed to determine the susceptibility of SAVY-4000 and Hagan containers to SCC. The boiling magnesium chloride test (ASTM G36) determined that Hagan container is susceptible to SCC in the region surrounding the TIG weld based on the cracking observed after 22-24 hours of exposure.[8, 10] No cracking was observed in the SAVY-4000 container, but a through-wall pit was found after 44-46 hours of exposure. Residual stress measurements obtained by the hole drilling technique (ASTM E837) indicate a hoop stress of 194 MPa in the Hagan container and an axial stress of 25 MPa in the SAVY-4000 container.[8, 11] These results show that Hagan containers are relatively more susceptible to SCC in the weld region than SAVY-4000 containers.

Further analysis of the SAI containers has found both pitting and cracking in the weld region. The conditions under which the pitting and cracking occurred are considered bounding of any container packaged for storage, yet these conditions did not result in a through-wall penetration. Because similar conditions could be reproduced in a laboratory setting, the SAI container content provided a basis for a set of accelerated aging studies. The test conditions in these studies can be controlled and allow the measurement of pitting and cracking rates as a function of time. Preliminary results from these studies are discussed in Section 4.0

2.0 Corrosion Observations in Storage

To date, 95 field surveillances have been performed. The surveillances included 50 SAVY-4000 container surveillances and 45 Hagan container surveillances. Additionally, 78 maintenance cycles have been performed on transfer containers. Corrosion was observed in 18 of the SAVY-4000 containers, and in 25 of the Hagan containers. Additionally, corrosion was found in three SAVY-4000 transfer containers packaged outside of the allowed content limits. A corrosion ranking scale and analysis was first implemented in the 2018 SAVY-4000 surveillance report [12]. The corrosion ranking scale was applied to all the SAVY-4000 containers from 2015 to 2019 and Hagan containers 2013 to 2019. Containers are assigned a group based on the overall appearance and coverage of the corrosion or coating. The group can be used to compare the corrosion behavior for various material forms and material types as well as to assess the progression of corrosion over time in containers that have repeating surveillances.

Table 1 defines the criteria for each corrosion group and gives the number of SAVY-4000 and Hagan containers in each group based on the criteria. Eight containers (five Hagan containers, one SAVY-4000 storage container, and two SAVY-4000 transfer containers) were assigned to corrosion group 3 based on the visual inspection. The conditions and packaging data for all containers assigned to corrosion group 3 are listed in Table 2. Photos of the worst containers observed to date are shown in Figure 1.

All of the containers assigned to corrosion group 3 had coatings on most or all of the interior surfaces. Most coatings on the inside surfaces consisted of dry powders or flakes, ranging in color from brown to white and removable by wiping with a wet cloth. Several containers had accumulated loose powder on the bottom of the containers. White powder was found on the outside of several containers. Several of the containers showed evidence that liquid had been present in the past or had liquid present at the time of opening. The inside surfaces of 18H7 (Figure 1e,f) were completely covered by a “gummy” residue that ranged in color from green to brown. The liquid was presumed to be plasticizer from the PVC bag mixed with corrosion product. Corrosion was found on the threads of five Hagan containers to date. The corroded threads of container 18H7 shown in Figure 1g resulted in the lid being fused to the container body. Three Hagan containers were found to have corroded threads in FY19 and are discussed later.

Table 1. Corrosion Group Descriptions and Number of Storage Containers Assigned by Group

Group	No. Containers SAVY | Hagan	Description	Criteria	Example
0	32 | 13	No Corrosion	No corrosion, staining, spots, or coatings observed	
1	9 | 7	Isolated General Corrosion	Corrosion, staining, spots, or coatings observed in isolated areas (e.g. corrosion found on weld only)	 17H2
2	8 | 11	Light General Corrosion	Corrosion, staining, spots, or coatings throughout container; light in overall density; bare metal visible	 15S10
3	1 | 7	Heavy General Corrosion	Corrosion, staining, spots, or coatings throughout container; heavy (dark) in overall density; little or no bare metal visible	 15H4
Note: No data are available for 7 Hagan containers.				

The worst appearing corrosion in any container to date was observed in 18H7 (Figure 1e-g). This container was originally chosen for surveillance in FY17, but surveillance could not be performed because the lid was fused to the body. In the interim, the Hagan was overpacked in a 3-Qt SAVY-4000 container for 14 months. In June 2018, the SAVY-4000 was unloaded, and the Hagan container was introduced into the glovebox line for opening. The lid was removed by making vertical cuts through the threads and prying the side of the lid to separate the threads of the lid from the body.

Table 2. SAVY-4000 and Hagan Storage Containers in Corrosion Group 3 (Containers 20T and 21T are the SAI SAVY-4000 transfer containers from FY16).

ID / Type / Size	Material Form	Nuclear Material Description	Age (y)	Power (W)	Visual Inspection	Comment
15H3 H 8-Qt	Dioxide	Plutonium, >19.00% Pu-240	5.6	5	• Sticky residue covering most inner surfaces	
15H4 H 8-Qt	Dioxide	Plutonium, 16.00 thru 19.00% Pu-240	11.5	10.5	• Corrosion and heavy coating covering most inner surfaces	
16H1* H 5-Qt	MSE Salt	Plutonium, 10.00 thru 13.00% Pu-240 (High Am-241)	8.1	2.9	• White powder on filter cover and on storage compartment • Wipeable coating covering inside surface	• White powder deposits outside container • 100-160 µm diam. pits by optical microscopy
16S8 S 8-Qt	Dioxide	Plutonium, 4.00 thru 7.00% Pu-240 Plutonium-238 (7%)	3.4	21.3	• Corrosion of TID wire and deposit of corrosion product on lid • Wipeable coating covering inside surface	•
18H7* H 1-Qt	MSE Salt	Plutonium, 4.00 thru 7.00% Pu-240 (High Am-241)	13	6.9	• Corroded threads; lid fused to body • Green-brown liquid covering inside surface	• 100-150 µm diam. Pits by optical microscopy
19H1 **H** **3-Qt**	Unalloyed Metal	Plutonium-242 > 60% (High Am-241)	18.1	14.9	• Corroded threads • Wipeable coating covering most of inside surface	
19H3 **H** **8-Qt**	Incinerator Ash	Plutonium-238	11.6	17	• Corroded threads • Corrosion outside filter • Wipeable coating covering most of inside surface	
19H5* H 1-Qt	MSE Salt	Plutonium, 4.00 thru 7.00% Pu-240 (High Am-241)	12.3	5.7	• Corroded threads; • Lid fused to body • Corrosion product powder covering walls and bottom	• 100-150 µm diam. Pits by optical microscopy
20T** S 5-Qt	Liquid; Chloride Solution	Plutonium; various	1.2	--	• White powder on lid surrounding filter • Corrosion product flaking off walls and covering bottom	• See SAI Container Case Study in Section 3.0
21T** S 5-Qt	Liquid; Chloride Solution	Plutonium; various	1.2	--	• White powder on lid surrounding filter • Corrosion product flaking off walls and covering bottom	• See SAI Container Case Study in Section 3.0

Abbreviations: S: SAVY-4000; H: Hagan; Qt: Quart
* Container introduced into glovebox line for unloading ** SAVY-4000 transfer container.

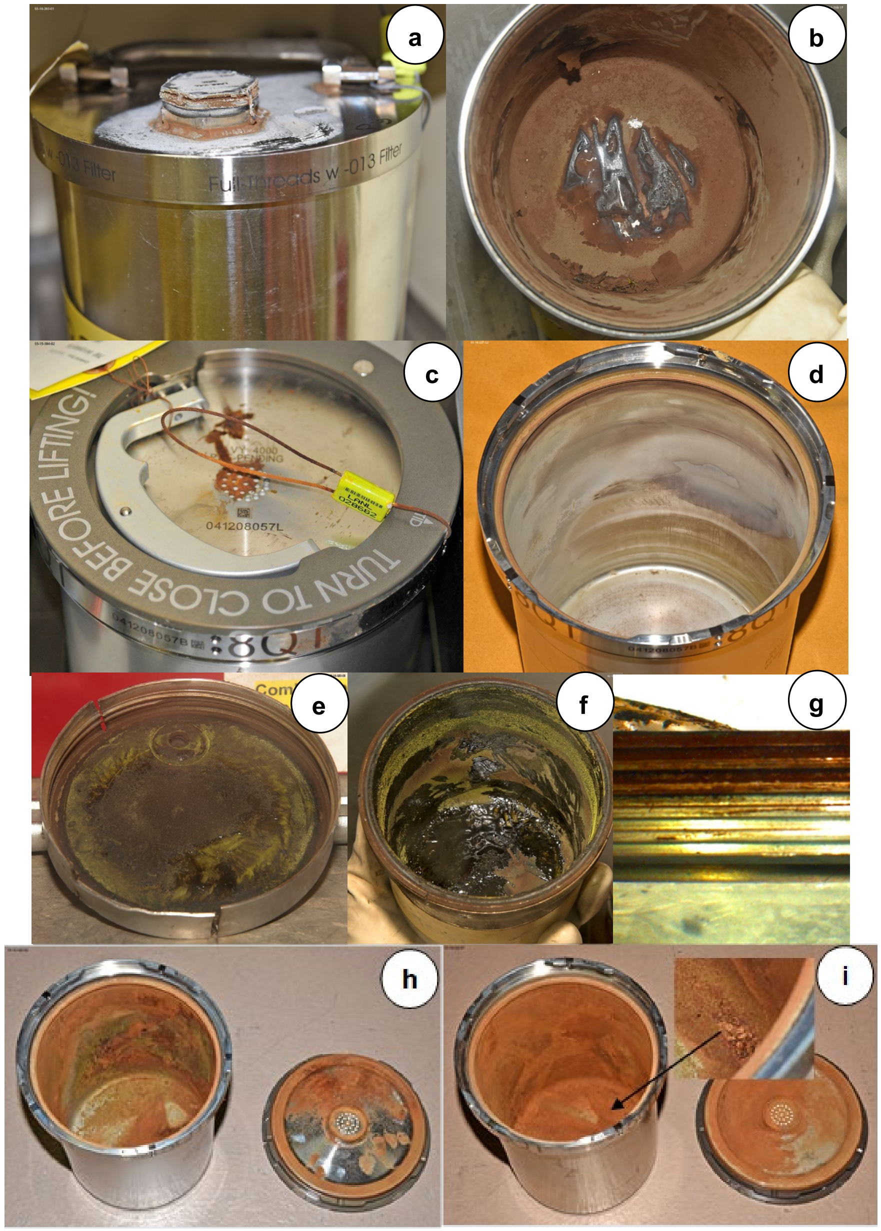

Figure 1. Photos of worst corrosion observed to date in SAVY-4000 and Hagan containers based on the visual inspection: (a) 16H1 lid with white powder deposit and corrosion on filter cap, (b) 16H1 inside surfaces have a brown coating, (c) 16S8 has corrosion product deposited on outside of lid from the corroded TID wire above, (d) 16S8 inside surfaces covered in brown and white powders, (e) 18H7 inner surface of lid covered in gummy, green-brown residue, (f) 18H7 inner surfaces of body with gummy, green-brown residue, (g) 18H7 corroded threads, (h) corrosion and loose brown powder on inside surfaces of 20T, (i) corrosion and loose brown powder on inside surfaces of 21T.

2.1 FY19 Corrosion Observations

The FY19 surveillance containers included ten SAVY-4000 containers and eight Hagan containers. The results are summarized in Table 3.

Table 3. FY19 Hagan Corrosion Observations

ID / Type / Size	Corrosion Group	Material Form	Nuclear Material Description	Age (y)	Power (W)	Visual Inspection	Comment
19H1 H 3-Qt	3	Unalloyed Metal	Plutonium-242 > 60% (High Am-241)	18.1	14.9	• Corroded threads • Wipeable coating covering most of inside surface	
19H3 **H** **8-Qt**	3	Incinerator Ash	Plutonium-238	11.6	17	• Corroded threads • Corrosion outside filter • Wipeable coating covering most of inside surface	
19H5 H 1-Qt	3	MSE Salt	Plutonium, 4.00 thru 7.00% Pu-240 (High Am-241)	12.3	5.7	• Corroded threads; • Lid fused to body • Corrosion product powder covering walls and bottom	100-150 µm diam. Pits by optical microscopy
19H7 H 1-Qt	2	Unalloyed metal	Plutonium, <4.00 Pu-240	17.5	1.5	• Spots of corrosion throughout body and lid (similar to liquid drops).	“Sister item to 19H7”
19IoOP45 H 5-Qt	0	MSE Salt	Plutonium, 16.00 < 19.00% Pu-240; (High Am-241)	10.8	4.4	• No corrosion	
19IoOP46 H 8-Qt	0	MSE Salt	Plutonium, 16.00 < 19.00% Pu-240 (High Am-241)	13.4	4.8	• No corrosion	
19IoOP50 H 5-Qt	1	Alloyed Metal	Plutonium, <4.00 Pu-240	17.5	1.5	• Corrosion on weld; • Bag residue on can bottom.	“Sister item to 19H7”
19IoOP55 H 5-Qt	2	MSE Salt	Plutonium, 16.00 < 19.00% Pu-240 (High Am-241)	12.7	3.7	• Light corrosion on body. Heaviest near collar and tack welds	

Corrosion was found on six of the eight Hagan containers in FY19. Three Hagan containers were assigned to corrosion group 3 and had corrosion on the threads of the container and lid. Hagan container 19H1 is shown in Figure 2. The container was packaged with a Pu-242 metal item. Contamination was found on the bag out bag, so the entire container was introduced. Sectioning and optical microscopy of this container is planned for FY20.

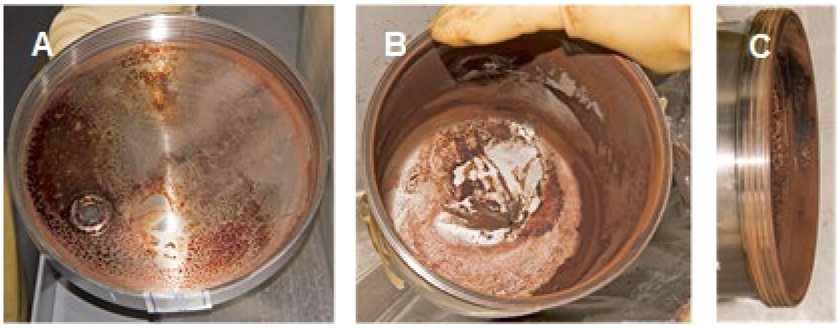

Figure 2. Hagan container 19H1 showing corrosion on lid (A), body (B), and the threads (C). Corrosion product powder was observed at the bottom of the container (B).

Hagan container 19H3 is shown in Figure 3. The container was packaged with a Pu-238 incinerator ash item. The entire container was introduced. Corrosion was found throughout the container as well as on the container threads and the outside of the filter.

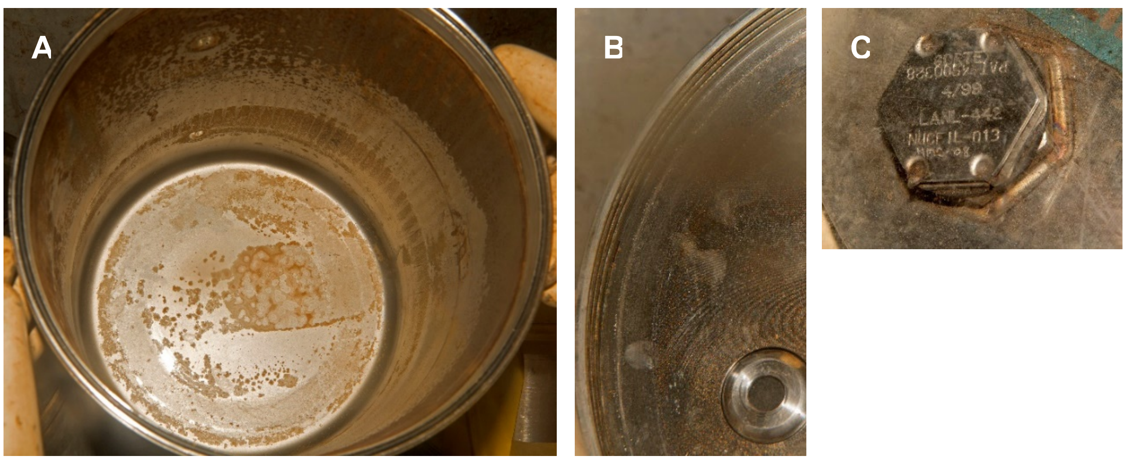

Figure 3. Hagan container 19H3 showing corrosion on lid (A), body (B), and the threads (C).

Hagan container 19H5 was selected for surveillance based on its similarity to container 18H7, which was the worst-appearing Hagan container observed to date. Details on container 18H7 are given in Figure 1e-g and Table 2. Both containers were 1-Qt Hagan containers packaged with MSE salt material. The conditions inside container 19H5 are shown in Figure 4. Similar to container 18H7, the lid of 19H5 was fused to the body due to corrosion. Therefore, the container was introduced into the glovebox line where it was opened by cutting. This container had heavy deposits of a brown powder covering the inside surfaces of the walls and lid and collected at the bottom of the container. The powder was removed from the container by brushing. The container was weighed before and after brushing and showed a weight difference of 4.2 grams due to removal of the powder. The identity of the powder was not determined but is believed to be mixture of stainless steel corrosion product and degradation product of the PVC bag. Optical microscopy was performed on sections of the cleaned container lid and body. The lid shows mostly general corrosion and shallow pits. The pit diameters could not be determined because much of the native surface was removed (Figure 4D). The container walls had large, agglomerated pits approximately 100 to 150 µm in diameter (Figure 4E).

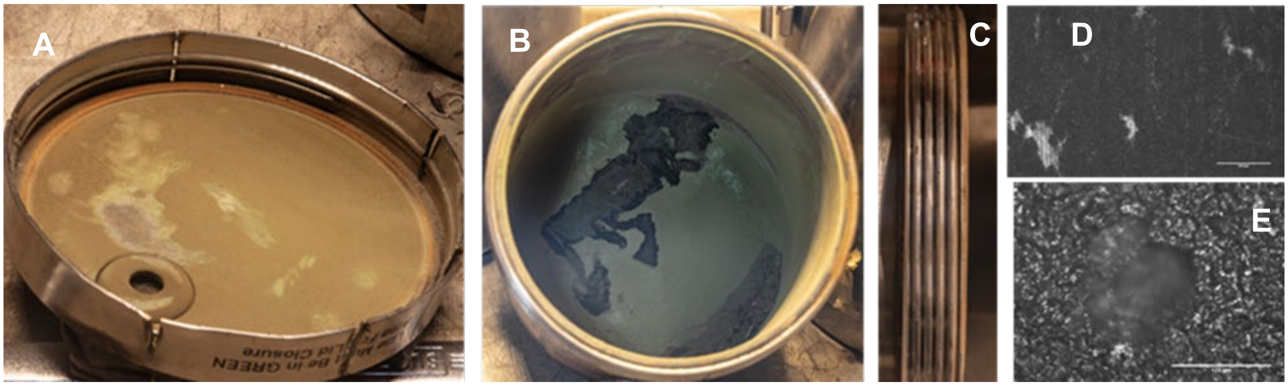

Figure 4. Hagan container 19H5 showing corrosion on lid (A), body (B), and the threads (C). Optical microscopy images show general corrosion (D) and pitting (E).

Two Hagan containers selected for surveillance in FY19 were both packaged about 17.5 years ago with identical contents in the same size Hagan containers. The history of their storage locations is not known at this time, but the items were retrieved from different shelf locations in the same PF4 vault room at the time of surveillance. Despite being packaged with the same contents, the two containers showed different corrosion behavior. Container 19H7 had spots of corrosion throughout the container giving the appearance of liquid droplets that had formed and later dried. Container 19IoOP50 only had corrosion in the weld region and bag residue on the container bottom.

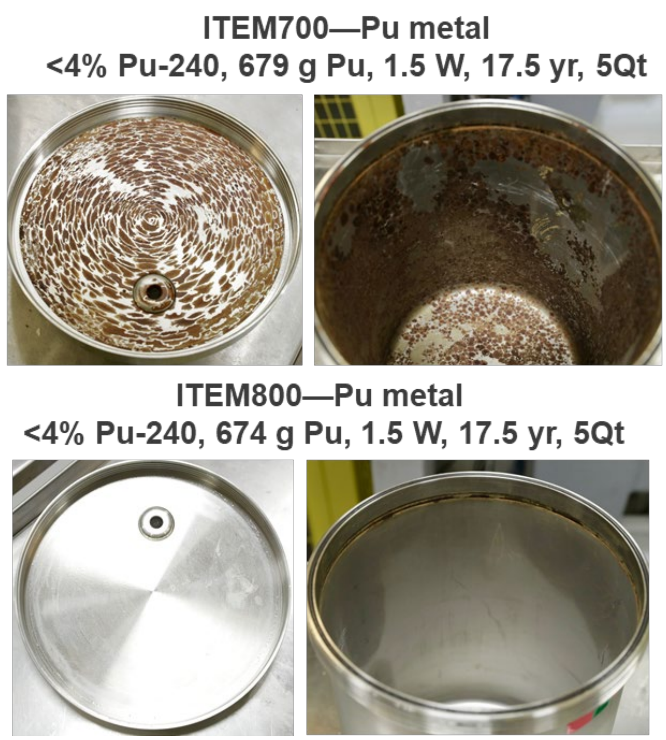

Figure 5. Comparison of 19H7 (top) and 19IoOP50 (bottom) packaged with identical content but stored in different vault locations.

Table 4. FY19 SAVY-4000 Corrosion Observations

ID / Type / Size	Corrosion Group	Material Form	Nuclear Material Description	Age (y)	Power (W)	Visual Inspection	Comment
19S1 S 8-Qt	2	Dioxide	Plutonium, >19.00% Pu-240	2.6	5	• Rust spots throughout container	APU bag samples placed inside can in FY18
19S2 S 5-Qt	0	Dioxide	Plutonium, 4.00 thru 7.00% Pu-240	6.3	2.1	• No corrosion	
19S3 S 3-Qt	1	MSE Salt	Plutonium, 4.00 thru 7.00% Pu-240 (High Am-241)	5.1	2.9	• Wipeable coating • White powder on filter	Bag out bag failed
19S4 S 5-Qt	1	Filter Residue	Plutonium, 4.00 thru 7.00% Pu-240	6.7	1.2	• Light deposits of corrosion on lower half of side wall	
19S5 S 8-Qt	0	Unalloyed Metal	Plutonium, 7.00 thru 10.0% Pu-240	3	0.2	• No corrosion	Contains capped inner SAVY-4000: 19S6
19S6 S 5-Qt	0	Unalloyed Metal	Plutonium, 7.00 thru 10.0% Pu-240	3	0.2	• No corrosion	Capped inner SAVY-4000 of 19S5
19S9 S 5-Qt	0	Sweepings /Screenings	Plutonium, 4.00 thru 7.00% Pu-240	6	2.73	• No corrosion • Liquid drops in container	
19S10 S 5-Qt	0	Salt	Plutonium, 4.00 thru 7.00% Pu-240	6	1.8	• No corrosion	
19S11 S 5-Qt	1	DOR Salt	Plutonium, 4.00 thru 7.00% Pu-240	6	2.8	• Rust spots on upper half of side wall and on bottom	
19S13 S 5-Qt	2	Dioxide	Plutonium, 16.00 < 19.00% Pu-240	3.5	10.5	• Rust spots throughout container walls and bottom	Bagout bag was black but pliable

Corrosion was found on five of the ten SAVY-4000 containers that had surveillance performed to date in FY19. The worst appearing containers were 19S1 and 19S13. The SAVY-4000 container 19S1 packaged with BLO-39-11-16 is shown in Figure 6. Corrosion is present throughout the container and heaviest in the region surrounding the weld. Surveillance has been performed on this container each year since FY17, and little change has been observed in the severity over that time frame (Figure 7). Samples of APU bag out bag material were placed inside the container in FY18 to test the behavior in a storage container. Because the samples were placed outside of the PVC bag out bag, they were exposed only to the thermal heat of the package and gamma dose. After one year, the bag samples show only slight yellowing.

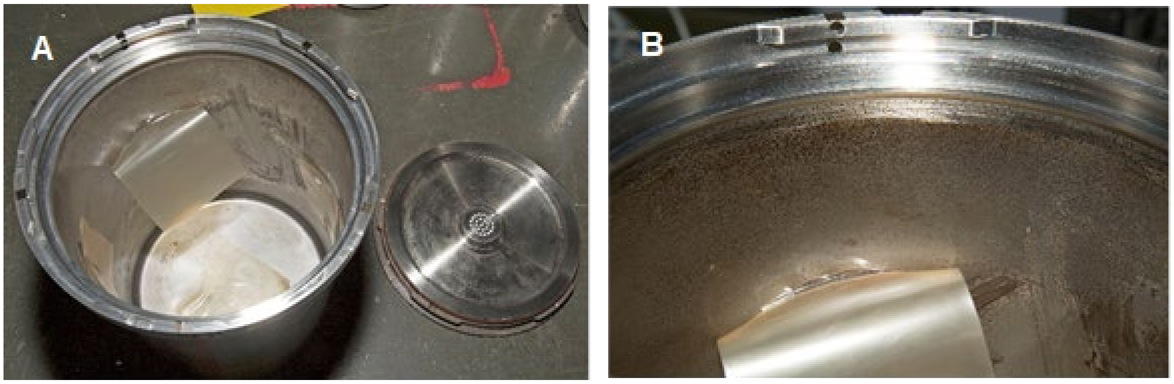

Figure 6. SAVY-4000 container 19S1 packaged with BLO-39-11-16. This container has spots of corrosion throughout the inside of the body and lid. Samples of the APU bag that were placed inside in FY18 show a slight yellowing.

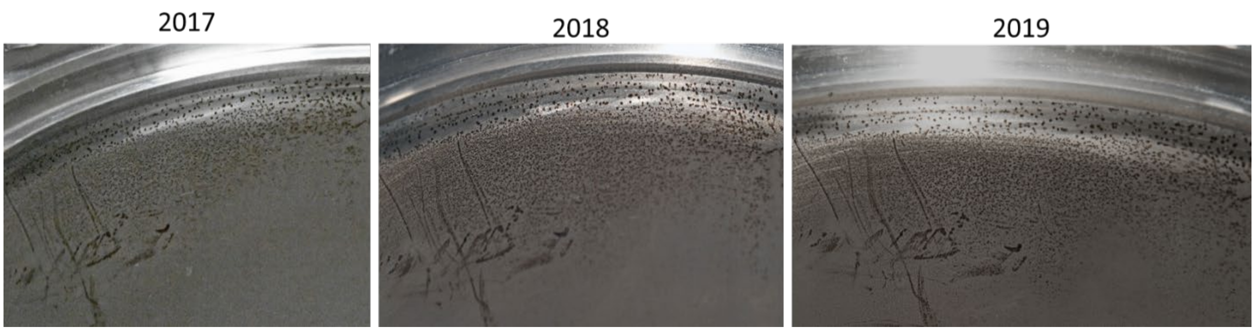

Figure 7. SAVY-4000 container 19S1 packaged with BLO-39-11-16 had surveillances performed in FY17, FY18, and FY19. Little change has been observed since FY17.

SAVY-4000 container 19S13 was packaged with an oxide material high in Pu-240 (16.00 < 19.00% Pu-240). Materials high in Pu-240 tend to be higher in Am-241, which increases the gamma dose to the PVC bag. As shown in Figure 8, the container has spots of corrosion on the lid and body as well as evidence of liquid residue and/or staining from the degradation of the bag. The bag was dark, but pliable. Due to concerns that the bag could fail during the next storage interval, a second PVC bag was added to the package.

Figure 8. SAVY-4000 container 19S13 showing corrosion on lid (A), body (B), and the dark-colored PVC bag out bag.

2.2 Trending Analyses

In an effort to guide the selection of future surveillance containers, corrosion trending analyses are used to relate various factors about the package itself to the corrosion observed in a package based on the corrosion ranking. The packaging factors include the age a of the package, the wattage w, and the container size (radius, r). A previous study has shown that a combination of these factors called the bag degradation factor (BDF) is related to the condition of the bag at the time the container is opened.[4] The BDF can be calculated as follows:

$$BDF = a * w/r^2$$

To evaluate trends between these packaging factors and the corrosion ranking, boxplots were created to show the wattage, age, and BDF as a function of corrosion category for the SAVY-4000 and Hagan containers. The boxplots are shown in the figures below.

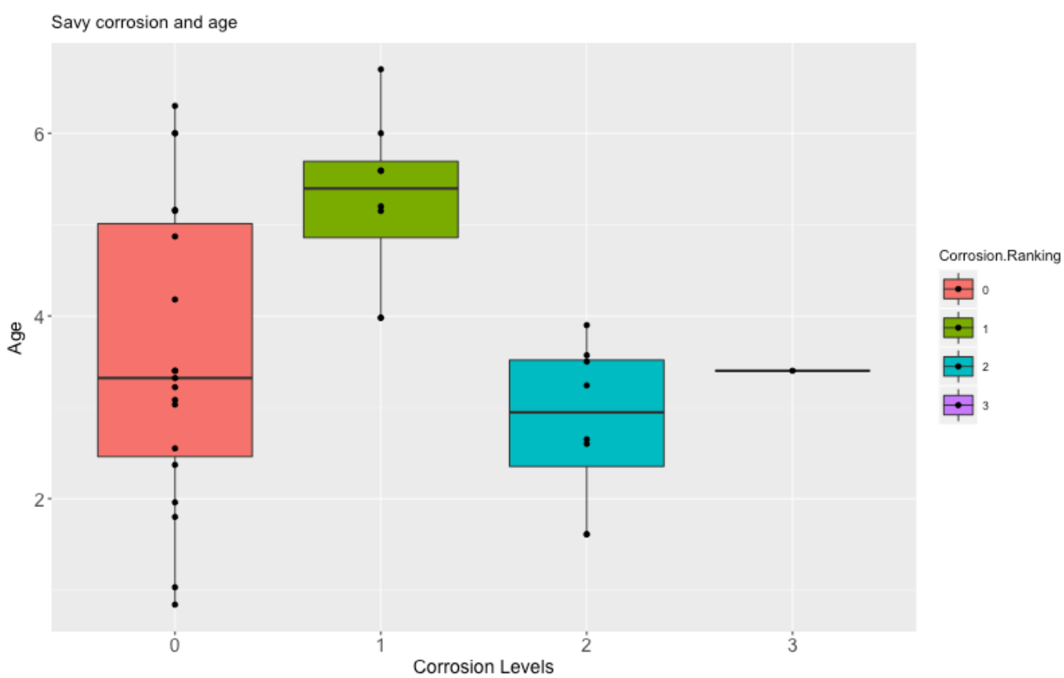

Figure 9. Boxplots of age versus corrosion rankings for the SAVY-4000 containers.

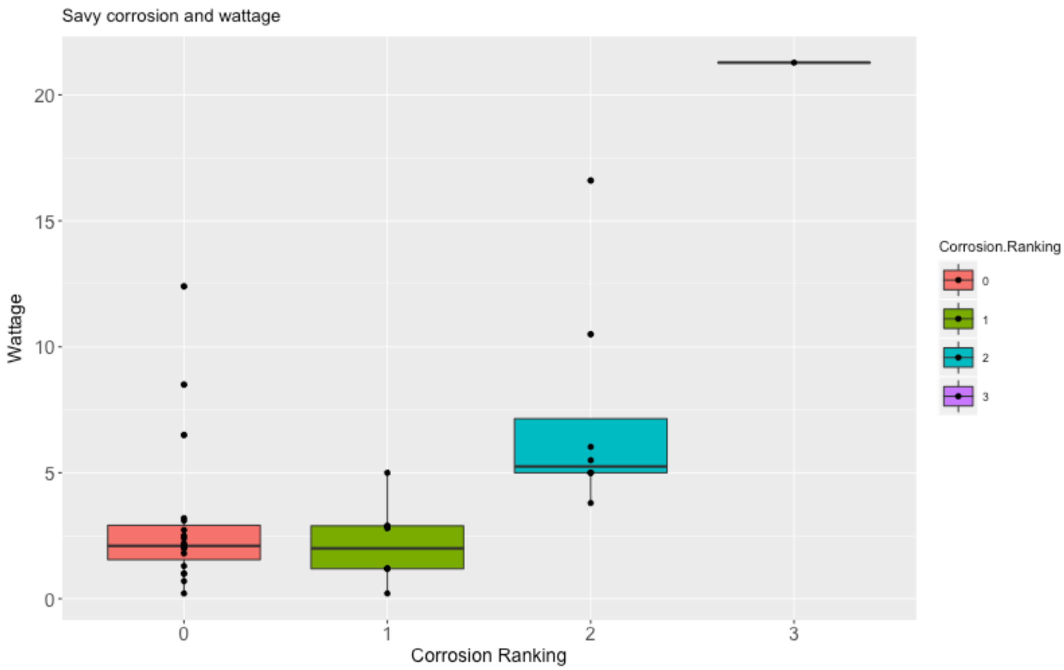

Figure 10. Boxplots of wattage versus corrosion rankings for the SAVY-4000 containers.

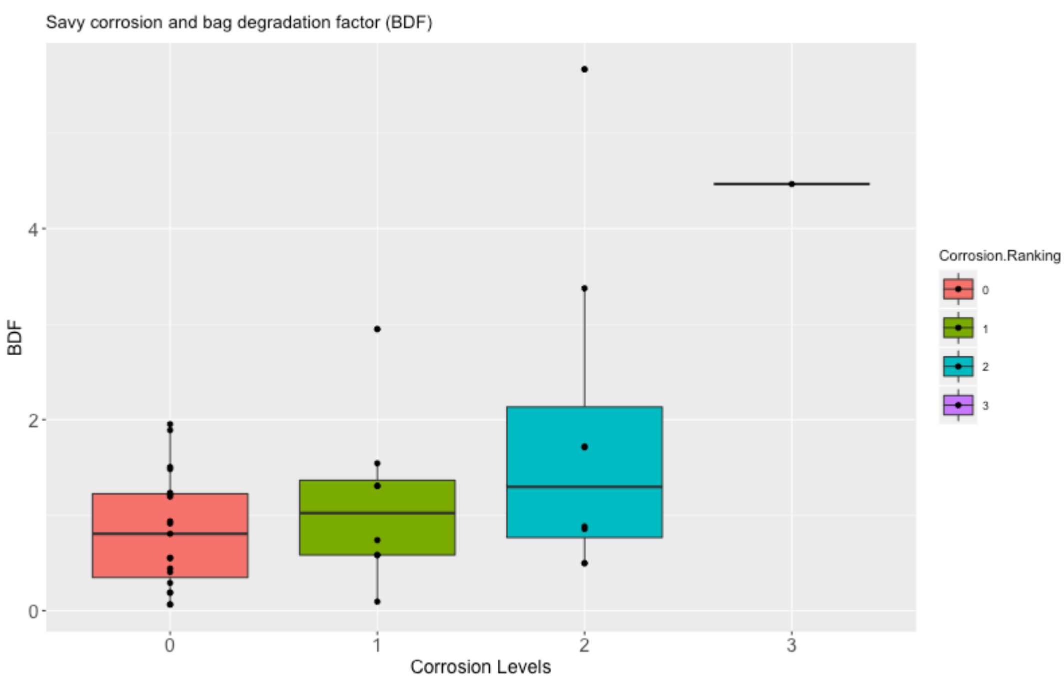

Figure 11. Boxplots of BDF versus corrosion rankings for the SAVY-4000 containers.

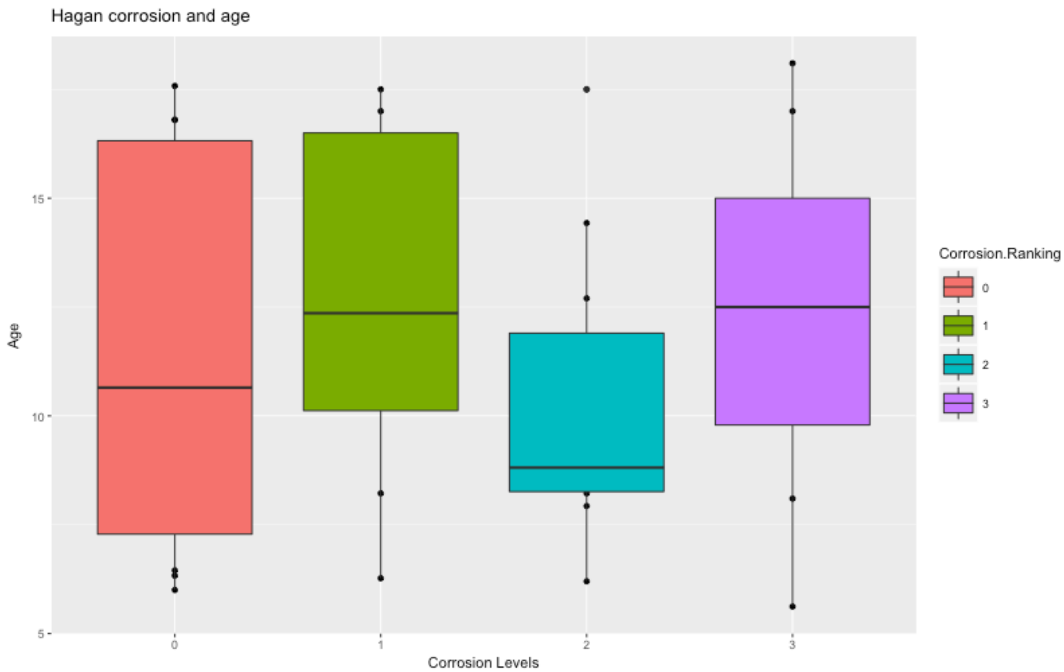

Figure 12. Boxplots of age versus corrosion rankings for Hagan containers.

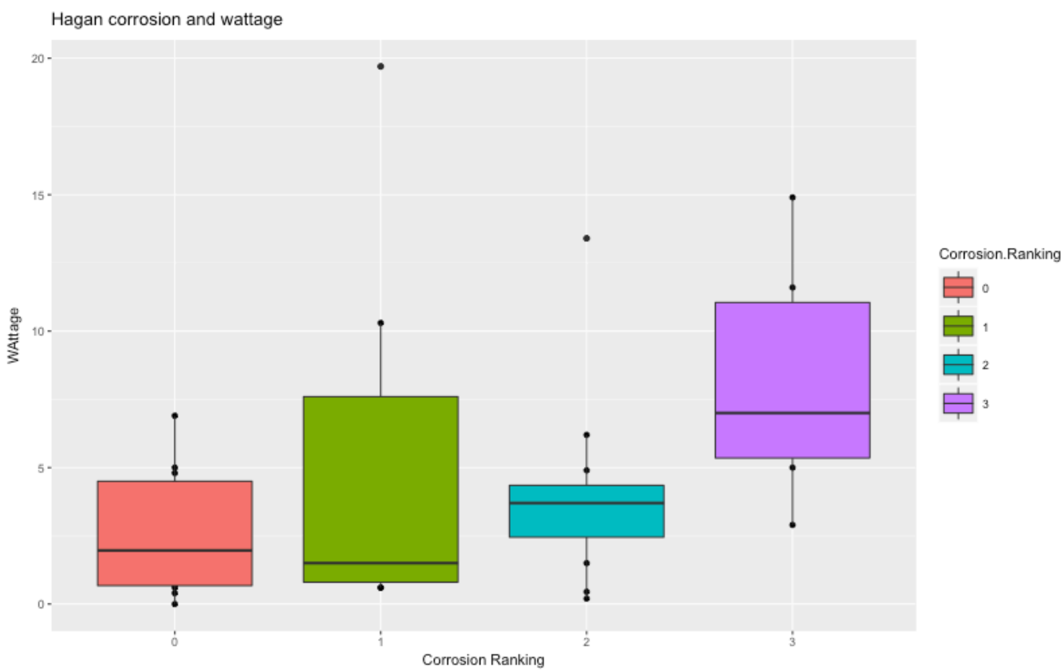

Figure 13. Boxplots of wattage versus corrosion rankings for Hagan containers.

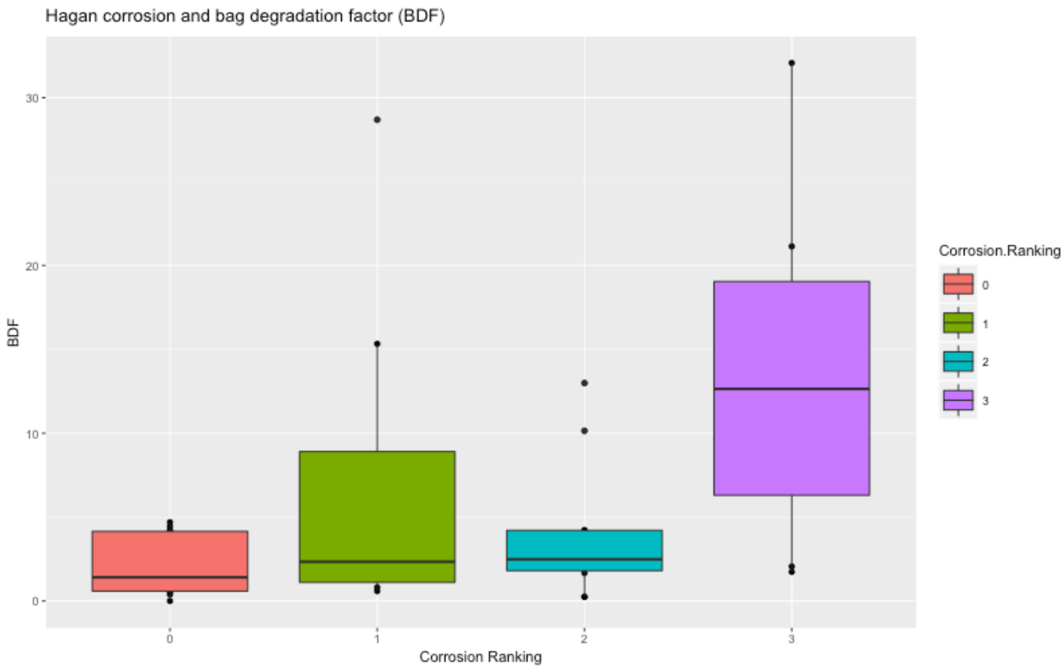

Figure 14. Boxplots of BDF versus corrosion rankings for Hagan containers.

The results do not show a trend between age and the corrosion ranking, but results show a weak trend between the corrosion ranking and the wattage and the BDF in both SAVY-4000 and Hagan container groups. The overlap between the groups suggests that other factors may affect corrosion behavior. As shown earlier, identically packaged Hagan containers (19H7 and 19IoOP50) and similarly packaged Hagan containers (18H7 and 19H5) stored in different locations showed different corrosion behavior. The differences suggest that environmental factors such as dose rate in the storage compartment, temperature, and relative humidity may have an effect on the condition of the storage container. Data for the environmental factors is not readily available, but future trending analyses could consider factors such as vault room and the proximity to the vault water baths as well as the average wattage of a storage compartment.

3.0 SAI Container Continuing Studies

This section summarizes the past and current analyses performed on the SAI SAVY-4000 containers. These containers were found to have the most severe corrosion, and the storage conditions are believed to be bounding those of any other storage container. Extensive analyses have been performed on these containers to better understand the effect of the storage conditions on the container integrity at bounding conditions.

3.1 Summary of FY17-18 Results

In FY16, two SAVY-4000 transfer containers used to store solution assay instrument (SAI) standards for approximately 14 months were found to have significant corrosion. [13] The SAI standards were packaged with solutions consisting of 0.1 to 200 g/L of Pu dissolved in 3M HCl contained within plastic Erlenmeyer flasks that were enclosed within a polyethylene (PE) plastic bag.[8] It is believed that the vapor from the solution was able to permeate the PE bags and exposed the inner surfaces of the SAVY-4000 to the corrosive gas.

The environment within the SAI containers is believed to be more severe than any conditions that could occur in a storage container due to the presence of an HCl solution and a high relative humidity (The relative humidity was estimated to be between 80 and 90% based on the water vapor pressure above a 3M HCl solution at room temperature. The HCl vapor pressure was approximately 0.01 Torr).[14] Therefore, it is reasonable to assume that these transfer containers will bound all conditions supporting corrosion in storage containers.

Photographs of the containers (Figure 15) show general corrosion after 14 months of use. Loose brown powder was found in the bottom of the container.[8] The exterior surface of the container lids had a deposit of white powder surrounding the filter. Samples of the brown and white powders were collected from each container. The brown powder collected from each container was weighed and found to have a mass of 1.9 grams. The remaining corrosion product was removed using Fantastik® cleaner on a piece of cloth. The cleaning did not require scrubbing and wiped clean.

20T 081305070 L/B	21T 011305020 L/B
	

Figure 15. Photos of SAI containers taken in FY16 for surveillance.

After cleaning the container, the laser etching was visible on the inside of the container wall (Figure 16). It appears that the laser etching caused a heat affected zone that, when exposed to HCl gas inside the container, caused a different corrosion effect in that area. Samples of the heat-affected zone were tested by exposing samples to $FeCl_3$, but the tests found no evidence that laser etching increased the susceptibility of the reverse side of Hagan or SAVY-4000 pieces when exposed to $FeCl_3$.

Figure 16. Image of laser etching on inside of container wall.

Analytical chemistry performed on samples of white powder collected from the outside surface of SAI containers as well as the brown powder collected from inside the SAI containers.[15] The identity of the white powder on the outside surface of the lid was determined to be ammonium chloride based on ion chromatography results. The brown powder was found to contain ammonium chloride and corrosion product of stainless steel based on ion chromatography and inductively coupled plasma mass spectrometry.

Both SAI containers had surveillance tests performed in FY17. The tests included a helium leak test, O-ring durometer measurements, filter penetration, and pressure drop across the filter. The containers passed all surveillance testing.[16] The containers were then removed from PF-4 for wall thickness measurements.[8] The measurement techniques included use of a coordinate measuring machine (CMM) and an ultrasonic test (UT) instrument. The measurements were performed on both SAI containers as well as an unused SAVY-4000 container. Both the UT measurements and measurements taken with the CMM indicated that no significant wall loss had occurred in the corroded SAI containers based on the comparison to an unused SAVY.

Although nondestructive testing did not show significant wall thinning, the corrosion working group recommended destructive testing due to concerns for through-wall pitting and cracking. Container 081305070 was selected for drop testing, and container 011305020 was selected for destructive evaluation using laser confocal microscopy. Drop testing was performed in a drop tower that is capable of drop up to a height of 15 feet 8 inches. [8] The drop tower was designed to allow containers loaded with a surrogate material to be dropped and have the particulate release measured using both an optical particle counter and by sweeping up the material that is distributed in the bottom of the tower. After drop testing container 081305070 four consecutive times, the post test leak rates were all below 1.0E-07 atm-cc/s (failure criteria 1.0E-05 atm-cc/s), and showed no change after each consecutive drop. Laser confocal microscopy is planned for the dropped container in FY20.

3.2 FY19 Laser Confocal Microscopy Results

This section describes the laser confocal microscope examinations of the SAI SAVY-4000 container that are currently underway and the preliminary results. Information in this section was taken from the following report:

Duque, J. G.; Hill, M. A.; Bohn, K.; Reeves, K. P.; Karns, T.; Rios, D.; Wendelberger, J. G.; Lopez, L.; Narlesky, J. E.; Kelly, E. J.; Kaufeld, K. A.; Vaidya, R.; Oka, J. M.; Stone, T. A.; Smith, P. H. Microscopic Characterization of Corrosion of SAVY-4000: SAI Container; LA-UR-19-28733; Los Alamos National Laboratory: Los Alamos, NM, 2019.

In FY19, SAVY-4000 container 011305020 was cleaned and sectioned to obtain approximately twelve 17 mm × 6 cm samples from the top of the container as shown in Figure 17.[17] The dashed yellow box in Figure 17A represents the approximate area of a single section.

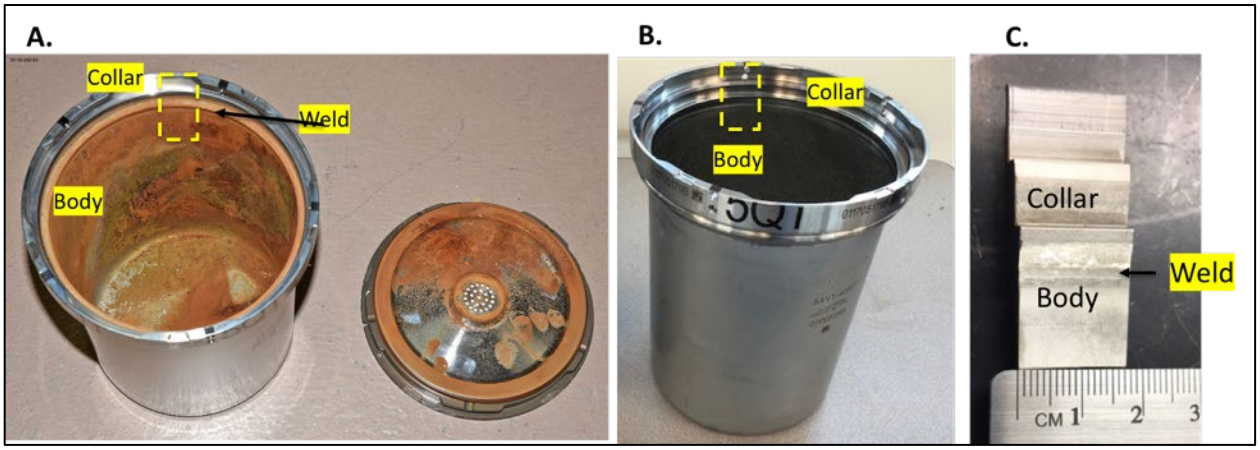

Figure 17. A. Photographs of container body after unloading. Picture taken from LA-UR-18-25709. B. Photographs of container body after cleaning. C. Small SAI section.

All surface images and surface depth profiles were obtained using a VK-X series Laser confocal Microscope (LCM) from Keyence (Figure 18). The system provides a non-contact, nanometer-level, 3-D profile and high-definition color images. Use of this technique to determine pit depth and density has been successfully demonstrated with the non-radioactive corroded samples.[18] Data was analyzed using the VK Analyzer software package V3.3 from Keyence and Origin® plotting software.

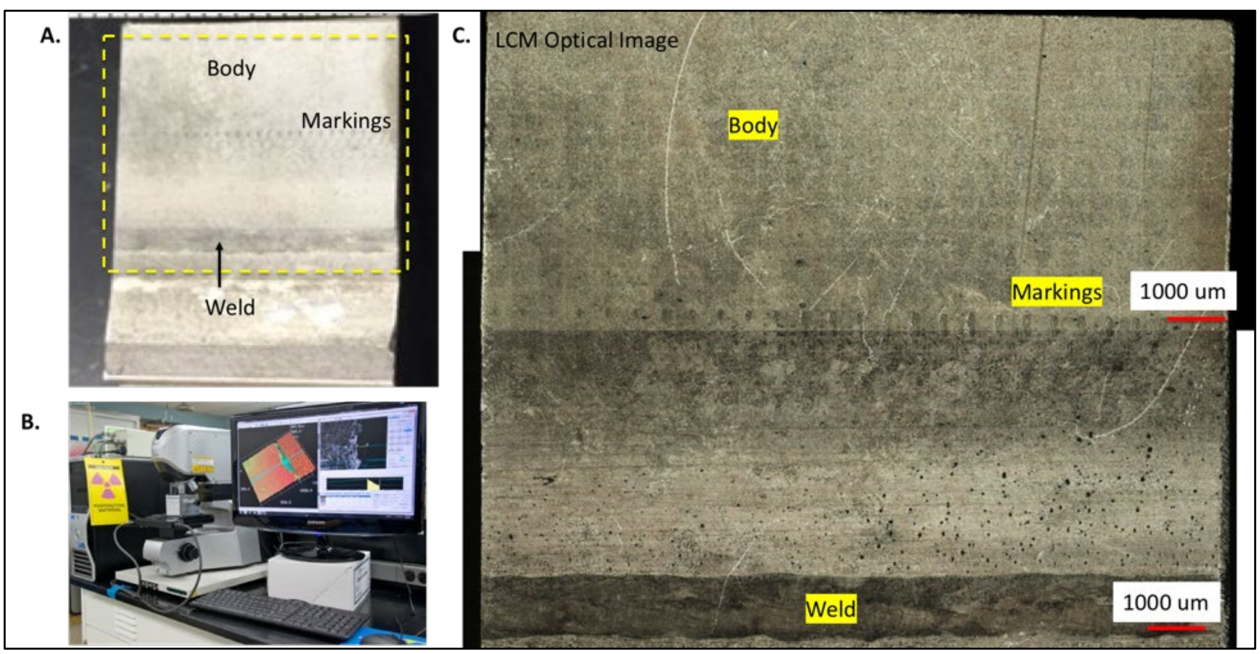

Figure 18. A. photograph of the characterized SAI section. B. Photograph of the Keyence Microscope. C. Surface image obtained with the Keyence instrument.

Cross sectional samples were obtained in order to examine sub-surface features in several regions of interest. The samples were mounted on an acrylic holder (Figure 19A) and the different locations were targeted for cross-sections starting from the body of the container toward the weld.

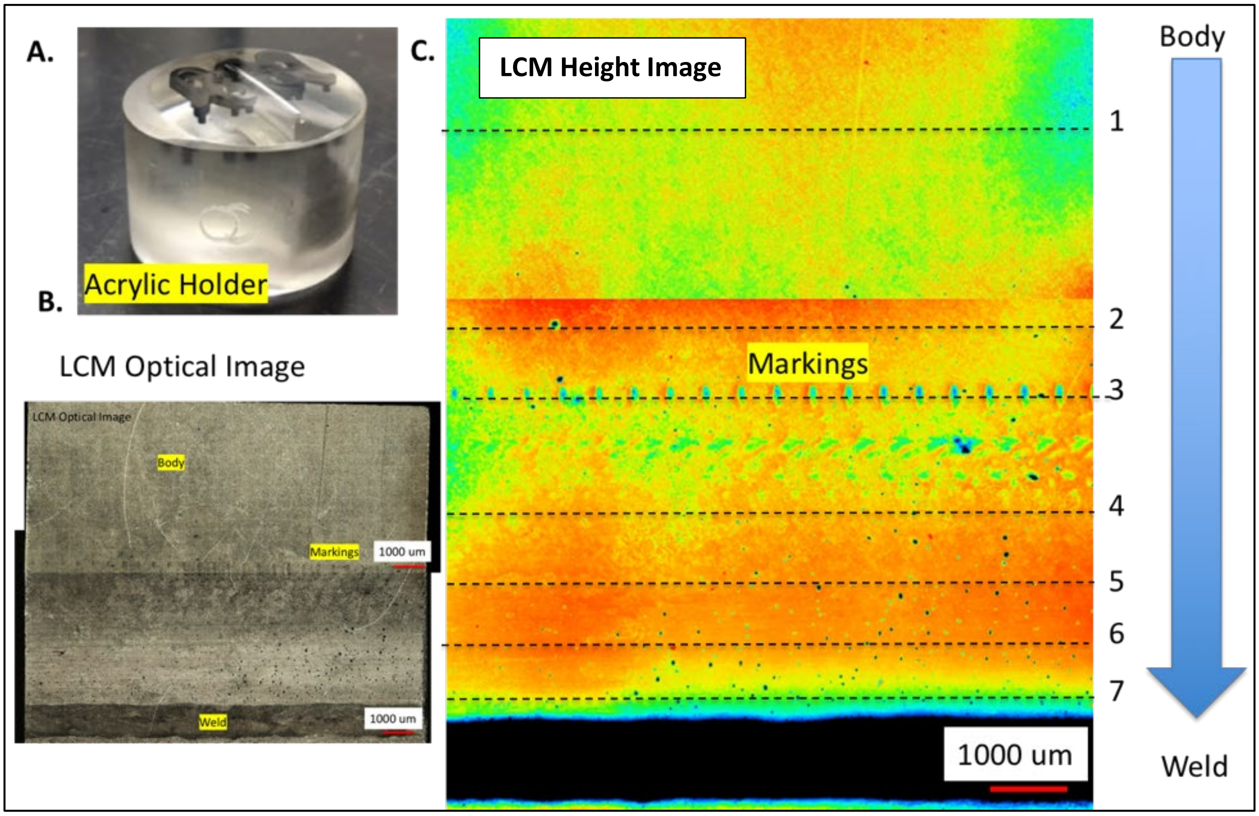

Figure 19. A. Photograph of the acrylic holder with the SIS section. B. LCM optical image of the SAI surface. C. LCM height image of the SAI sample with the pre-determined areas where cross-sectional analysis was performed.

Examination of the height data collected on the surface of the SAI sample (Figure 19c) found pitting with a pit depth distribution ranging between 5 and 60 microns (Figure 20). The region with the highest density of pits is located near the weld, as shown in Figure 19.

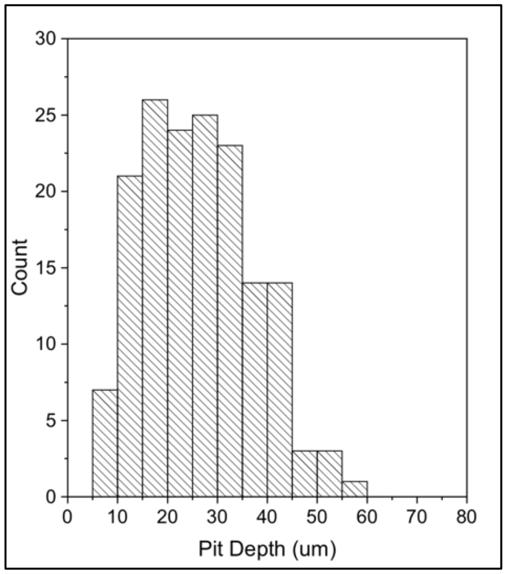

Figure 20. Pit depth statistics of SAI section.

Close examination of the pits shows that the pits further from the weld were round in shape while the pits nearest to the weld were elongated in the vertical direction. Figure 21 shows some representative profiles for rounded and elongated pits. The aspect ratio between the width and length of round pits shows a value close to one while the aspect ratio for elongated pits is less than 0.5 (Figure 21d).

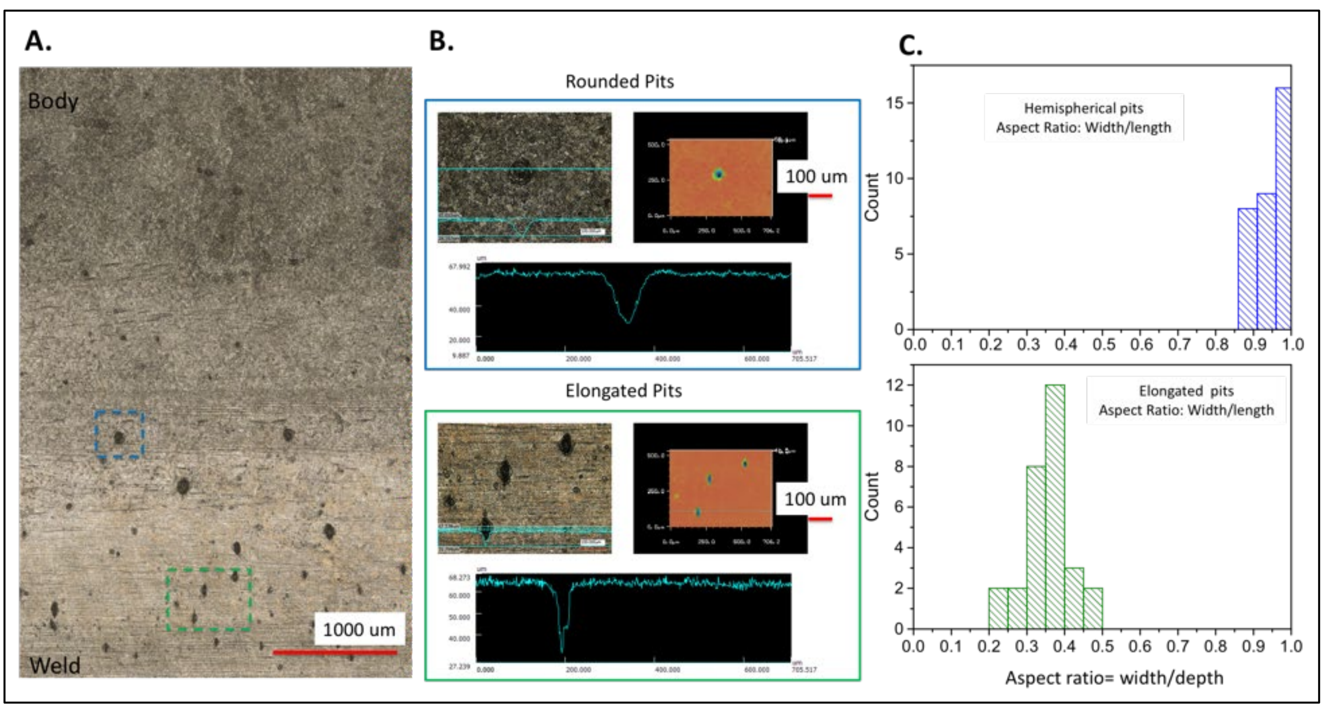

Figure 21. A. Representative optical image of different pits. B. Height profile for rounded pits and elongated pits. C. Histogram of the aspect ratio between the width and length of the pits for rounded and elongated pits.

A critical aspect of this work is to develop correlations between the surface image and sub-surface profile. Figure 22 shows the relationship between the surface image with unique markings on the surface of the sample, and cross section sample 3 as shown in Figure 19. A good correlation was observed between the surface features and the sub-surface features, which include shallow pits up to approximately 10 microns in depth and 140 microns wide shown in the black and orange boxes below. Interestingly, the sub-surface profiles reveal some small cracks at the bottom of these markings. The origin of these markings is unknown and are only seen in this container. At this time it is impossible for us to know if these cracks were a result of the corrosion or the marks themselves.

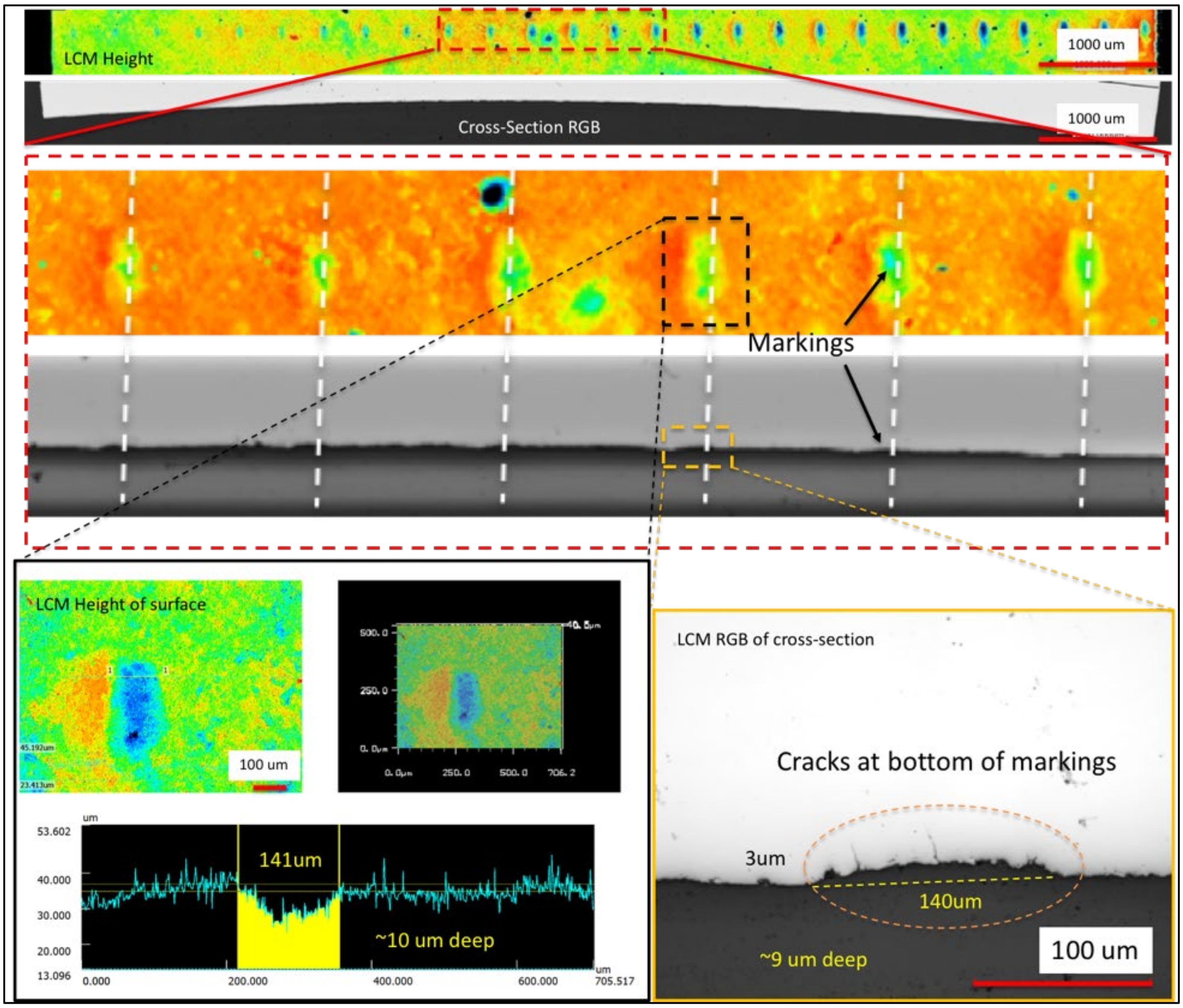

Figure 22. Representative LCM ensemble images of the surface (height data) and cross-section (sub-surface). Red dotted box is a zoom of the ensemble to highlight correlations. Black and orange boxes are higher resolution images of the ensemble to show small features profiles.

A representative correlation between the surface and the cross section is shown in Figure 23. Mild surface corrosion is observed on the body of the container (cross section samples 1 through 4) with a small number of rounded pits. Between cross section samples 4 through 6 a higher density of rounded pits was observed. At approximately cross section sample 6, the pits become elongated in shape. The elongated pits have a triangle-like shape with small cracks at the bottom of the pits. The cracks are transgranular in nature. No through-wall cracks were found.

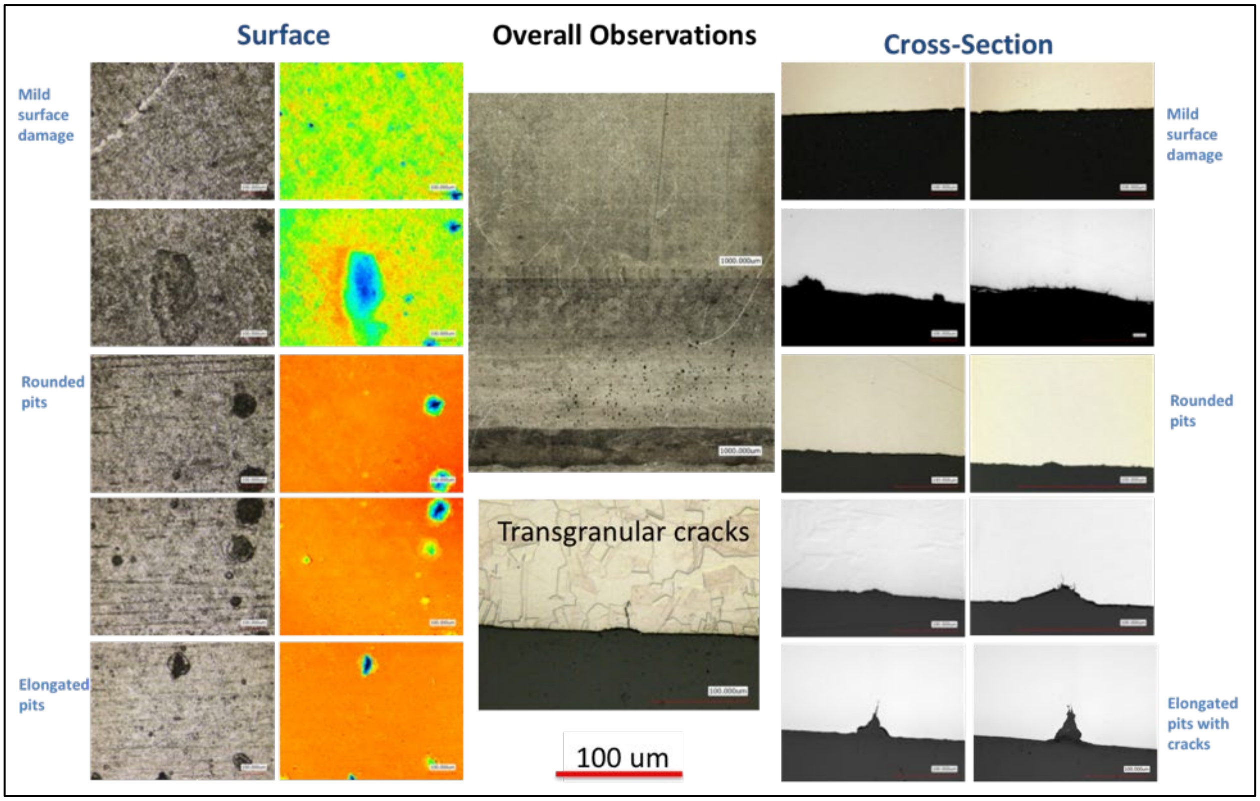

Figure 23. A. Representative images of the surface and cross-sections at different cross-section points. All images collected with LCM instrument.

The aspect ratio (width/depth) of the pits in Figure 23 was measured using LCM images. The measurements show that the width of pits without cracks is 4 times that of the depth. Pits with cracks have a smaller aspect ratio. Figure 24C shows a graph of the depth versus the width shows a nearly exponential increase in the depth due to the cracks. These results suggest that the pits that have cracks at the bottom of the pits nearest the weld are getting deeper at a much faster rate than those away from the weld.

The distribution of the crack lengths (measured from the bottom of the pit) and feature lengths (pit plus crack) was obtained. The distribution shows that the crack lengths range from 5 to 40 microns long while the depth of the overall features ranges from 5 and 80 microns (Figure 25). The maximum depth of the overall features is approximately 10 percent of the SAVY-4000 container wall thickness.

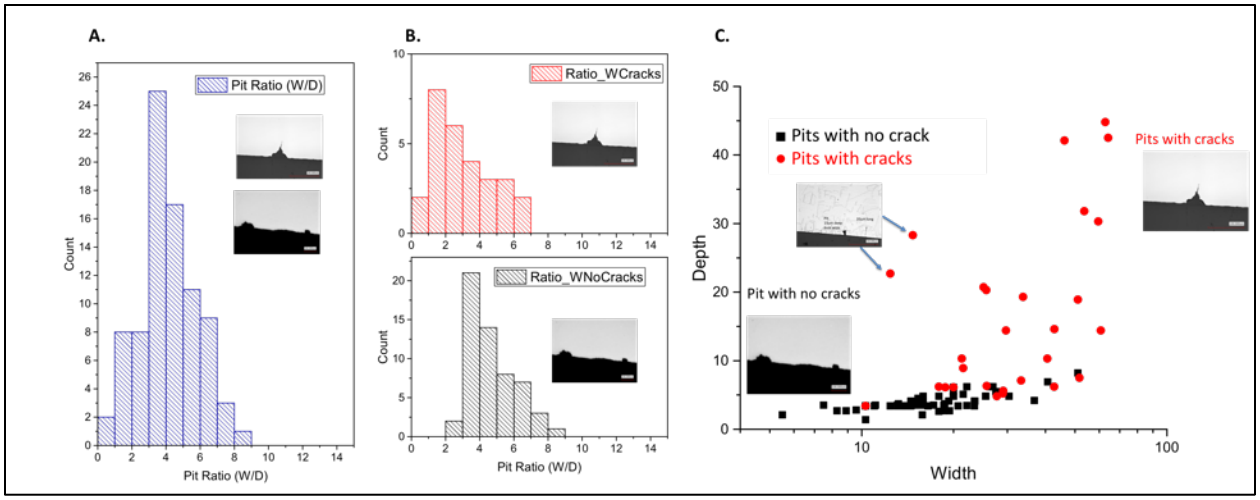

Figure 24. A. Width/depth aspect ratio for all pits. B. Width/depth aspect ratio histogram for pits with cracks (red) and pits without cracks (black). C. Correlation between depth and width for the pits with cracks (red) and pits without cracks (black).

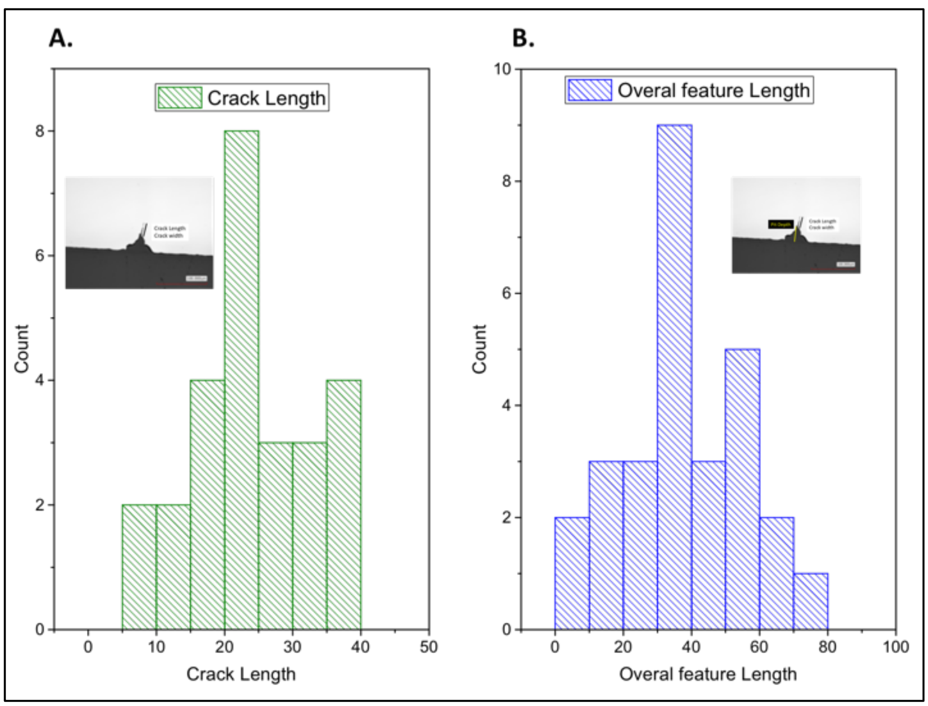

Figure 25. A. Histogram of the crack lengths from the bottom of the pits. B. Histogram of the entire feature length, pit plus crack.

The results of these analysis shows that exposure to HCl gas in a high humidity environment (>80% RH) resulted in pitting. A higher density of pitting was found near the weld region of the container body. The depth of the pits based on the surface examination ranged from 5 to 60 microns. The pits nearest the weld were elongated in shape. Additionally, elongated pits also have small crack-like features. The crack lengths range from 5 to 40 microns long while the depth of the overall features ranges from 5 and 80 microns. These results suggest that the heat affected zone associated with the weld is the most susceptible area for stress corrosion cracking.

4.0 Accelerated Aging Studies

This section describes the accelerated aging studies that are currently underway and the preliminary results. Information in this section was taken from the following report:

Rios, D.; Duque, J.; Wendelberger, J. G. *Accelerated Corrosion Studies with SAVY-4000 and Hagan Containers*; LA-UR-19-28711; Los Alamos National Laboratory: Los Alamos, NM, 2019.

The primary objective of the accelerated aging studies is to determine the potential of pit and crack growth rates between the two containers when exposed to HCl gas, which has been identified as the primary gas causing internal corrosion in packaged SAVY-4000 and Hagan containers.[19] The test conditions in these studies can be controlled and can allow the measurement of pitting and cracking rates as a function of time.

A set of experiments were conducted on a 5-Qt SAVY-4000 container, a 5 Qt Hagan container, and test specimens of both types of containers. The containers were instrumented with relative humidity sensors to record the humidity inside the container throughout the experiment, and the container lids were modified by plugging the filters to prevent the release of HCl vapors. Corrosion test specimens were obtained by cutting pieces from additional SAVY-4000 and Hagan containers. The test specimens include a portion of the include wall, weld, and collar regions.

The interior of the SAVY-4000 and Hagan containers as well as the test specimens were exposed to 150 mL of 6M HCl held within a 500 mL volumetric flask setting on the container bottom. The solution controlled the relative humidity in the SAVY-4000 container at 65% RH, and 62% RH in the Hagan container. The containers were opened and corrosion test specimens were removed from the containers after 31, 63, 95, and 126 days of exposure to HCl vapors. After removal of the last corrosion sample, the containers continued to be exposed to HCl vapors for an additional 42 days for a total exposure time of 168 days. The corrosion specimens were then photographed, cleaned, and analyzed by laser confocal microscopy. Photographs of the test setup before exposure are shown in Figure 26. Photographs of the containers after exposure are shown in Figure 27 and Figure 28.

Figure 26. Photographs of SAVY-4000 (A, C) and Hagan (B, D) storage containers enclosing 150 mL of 6.0M HCl in a 500 mL Erlenmeyer flask and four corrosion specimens (SAVY-4000and Hagan wall/collar pieces, respectively). Container lids were instrumented with a relative humidity sensor to record the relative humidity inside throughout the experiments. Filters on the lids were plugged to prevent the release of HCl gas.

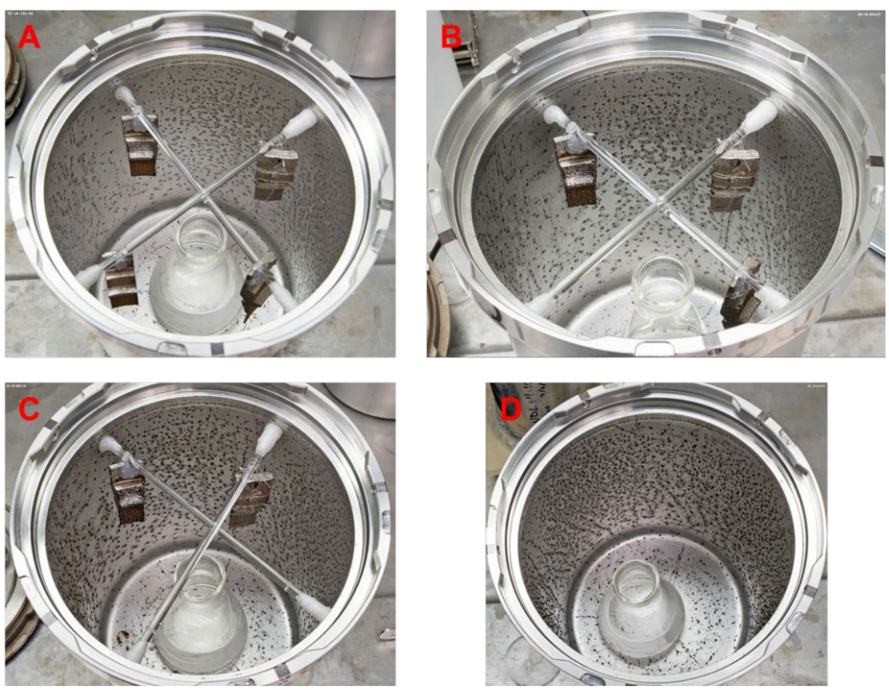

Figure 27. Photographs of SAVY-4000 storage container after exposure to the vapors from 6.0M HCl for 31 (A), 63 (B), 95 (C), and 126 (D) days. Photographs show an increase in corrosion density on the container wall with increased exposure time. Similar corrosion behavior was observed on the container lid (photographs not shown).

Figure 28. Photographs of Hagan storage container after exposure to the vapors from 6.0M HCl for 31 (A), 63 (B), 95 (C), and 126 (D) days. Photographs show an increase in corrosion density on the container wall with increased exposure time. Similar corrosion behavior was observed on the container lid (photographs not shown).

For the SAVY-4000 container, an increase in corrosion density was measured on the container wall with increasing exposure time. The corrosion is isolated to corrosion "islands" and does not cover the entire surface of the container, and it is not greater at the weld area. Similar corrosion was also observed in the exposure of teardrops (stainless steel samples) to 6.0M HCl vapors.[20] The corrosion observed on these SAVY-4000 container test specimens is shown in Figure 29. These samples also have isolated corrosion "island" and general corrosion covering the entire surface of the sample, which was not observed on the container wall. Surface analyses after cleaning found surface corrosion and uniform pitting on the entire surface of these samples (Figure 30). Increasing exposure time to HCl vapors did not significantly result in an increased number of pits on these samples, and only a small increase in pit depths was measured.

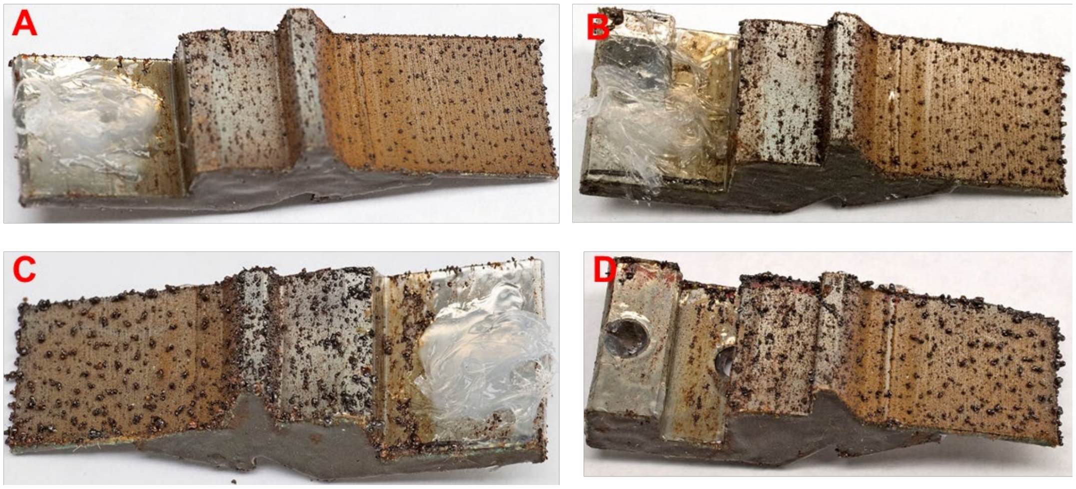

Figure 29. Photographs of SAVY-4000 corrosion specimens after exposure to vapors from 6.0M HCl for 31 (A), 63 (B), 95 (C), and 126 (D) days. Photographs show the presence of corrosion "islands", present in the container, and general corrosion. The latter was not observed on container walls.

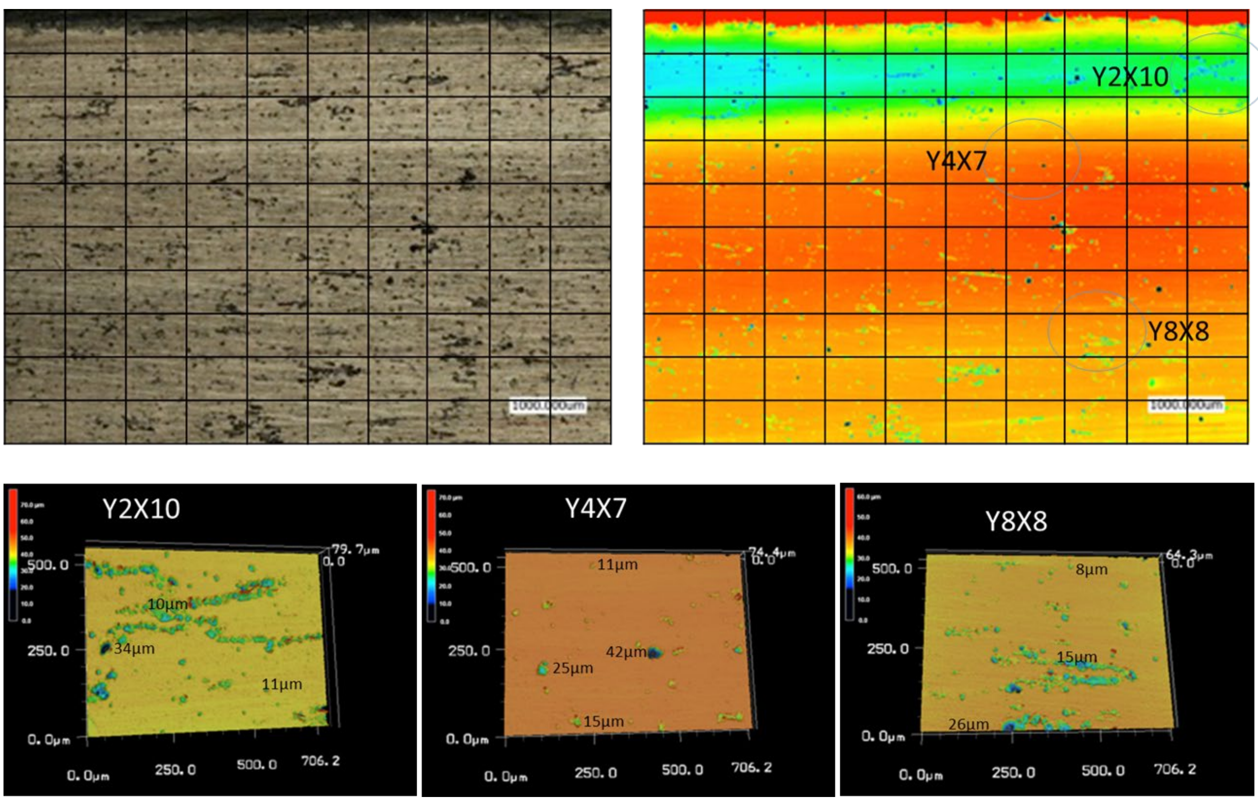

Figure 30. Representative optical stitched (top left) and height stitched (top right) images (10x10) of the SAVY-4000 corrosion specimen exposed to vapors from 6.0M HCl for 31 days. Images show a uniform pit distribution. Height images (bottom) show isolated and agglomerated pits of different depths. The remaining corrosion specimens have similar uniform pit distribution (images not shown).

Similarly, a Hagan container and four corrosion specimens were exposed to the vapors from 6.0M HCl. The photographs show an increase in corrosion density on the container wall with increasing exposure time. The corrosion is also isolated to corrosion "islands" but in this case, there is more surface coverage compared to the SAVY-4000 container. Surface analyses by LCM on the container wall are currently ongoing. The Hagan container test specimens showed similar corrosion to what was observed on the container (Figure 31). Surface analyses after cleaning found surface corrosion, and pitting on all of the samples, with corrosion cracks observed on the samples removed after 95 and 126 days of exposure. The pits and cracks were observed in the heat-affected zone (Figure 32). Increasing the exposure time in these samples increased the number of pits, and the pit depths as shown in Figure 33.

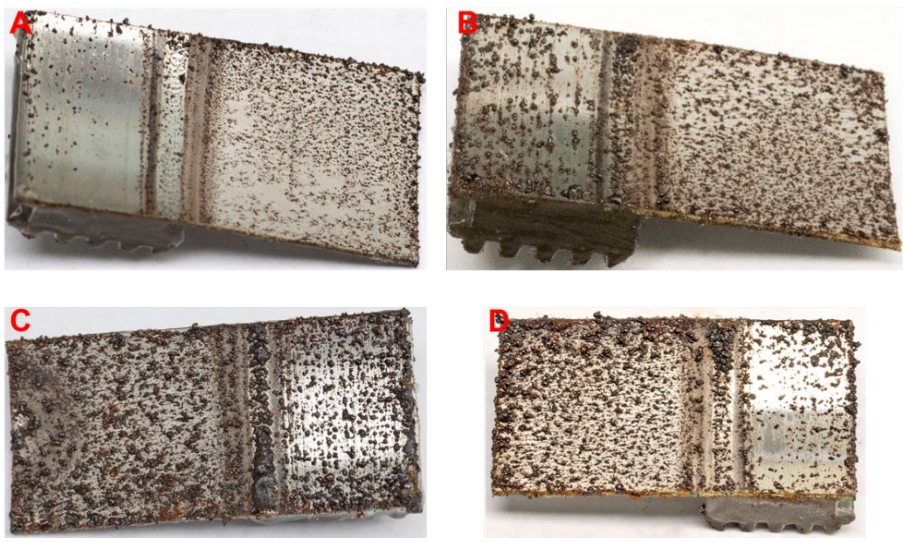

Figure 31. Photographs of Hagan corrosion specimens after exposure to vapors from 6.0M HCl for 31 (A), 63 (B), 95 (C), and 126 (D) days. Photographs show the presence of corrosion "islands" which are also present in the container.

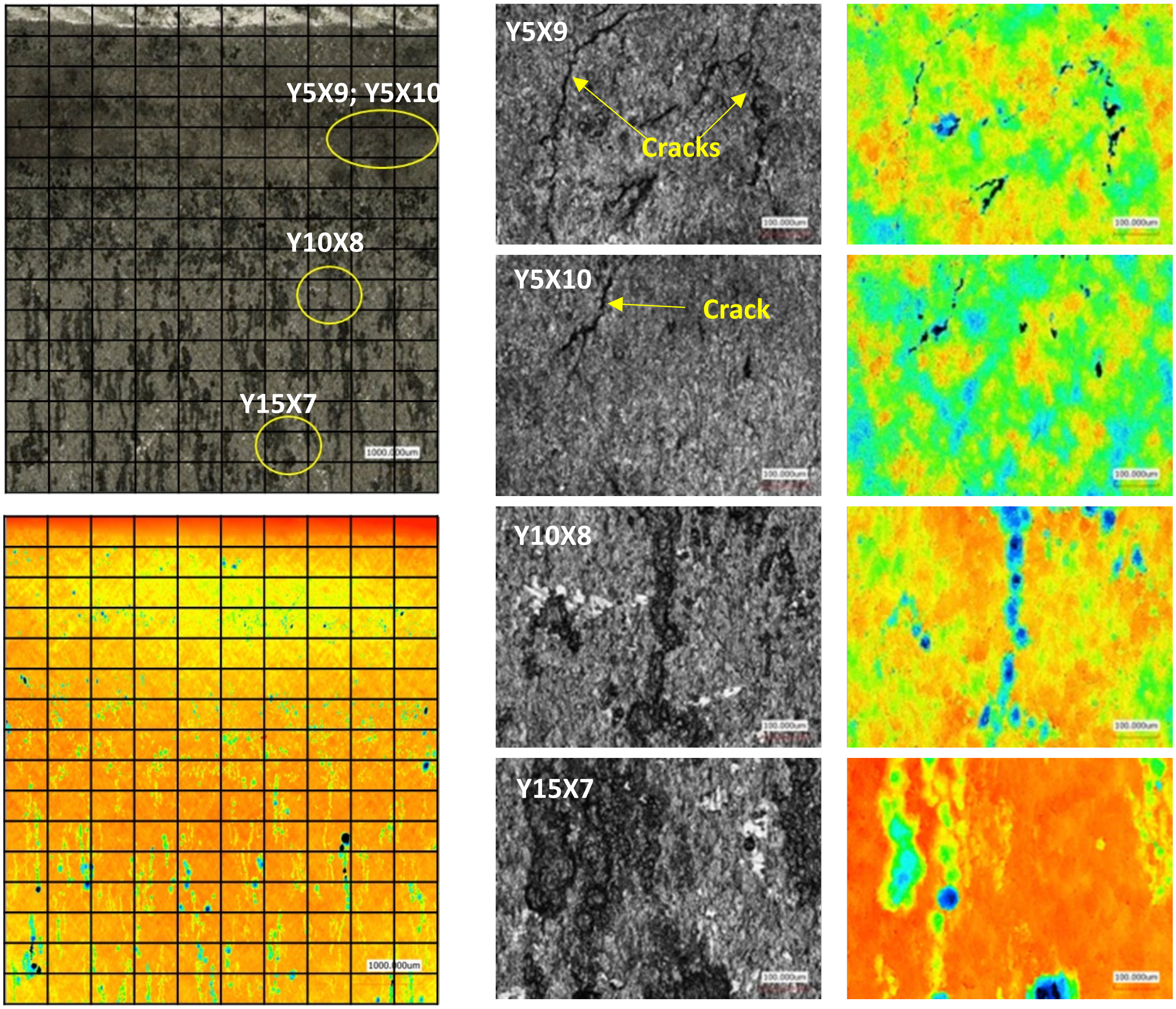

Figure 32. Representative optical stitched (top left) and height stitched (bottom left) images (10x16) of Hagan corrosion specimen exposed to vapors from 6.0M HCl for 126 days. Optical (middle) and height (right) images show the presence of cracks (Y5X9; Y5X10) and pits (Y10X8; Y15X7) on this sample.

Preliminary results from these studies seem to confirm that Hagan containers are more susceptible to pitting and cracking when exposed to HCl in a moist environment based on the observations of cracking in the Hagan container test specimens. Additionally, Hagan containers have higher rates for pitting than SAVY-4000 containers under the same conditions as shown in Figure 33.

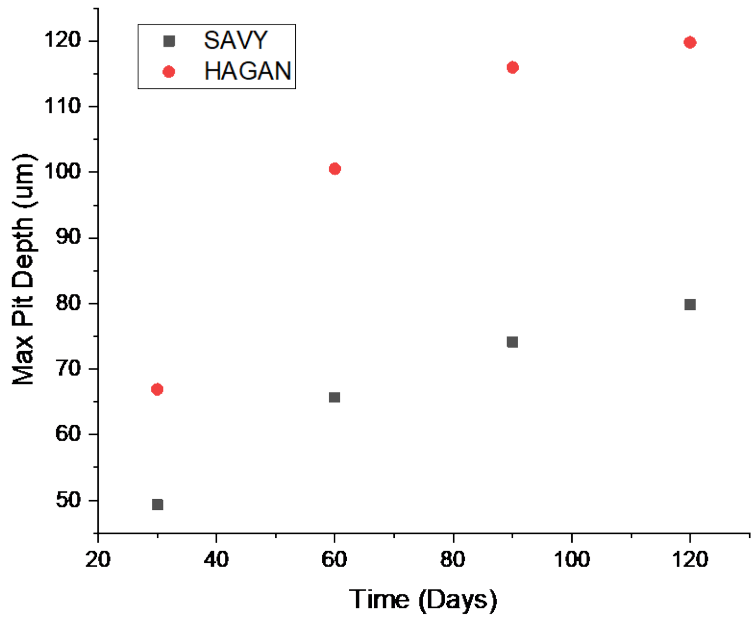

Figure 33. Maximum pit depth of SAVY-4000 (black squares) and Hagan (red dots) as a function of time for container test specimens.

5.0 PVC Bag Replacement

This section was contributed by Joseph Dumont and describes the recent efforts to understand PVC degradation and find a suitable material for use in bag out bags. Additional details can be found in the following reports:

Dumont, J. H.; Crum, S. L. A.; Zhao, C.; Murphy, E. C.; Reardon, S. D.; Lee, S. Y.; Lee, K.-S.; Labouriau, A.; Karns, T.; Smith, P. H. *Functional Testing of Alternative Bag-Out Bag for PF-4 Implementation*; LA-UR-18-25708; Los Alamos National Laboratory: Los Alamos, NM, 2018.

Dumont, J. H.; al., e., Aging of Aromatic Polyurethanes Bags for Nuclear Storage. *Transactions of the American Nuclear Society* **2019,** *120*, 417-418.

Dumont, J. H.; al., e., Effects of thermal aging and ionizing radiation on sPVC and aromatic polyether urethane used to store nuclear materials. *Polymer Testing* **2019,** *78*.

PVC is a thermoplastic that exhibits low flammability and resistance to acidic and alkaline environments[21]. Incorporation of plasticizers like phthalate esters turns PVC into a compliant material ideal for the manufacturing of plastic bags[21a, 22]. Di-n-octyl phthalate (DOP) is one of the most commonly used plasticizers with PVC, which can represent as much as 40% by weight of the PVC bag [21a, 23]. These large amounts of plasticizer may become problematic over time because, depending on environmental conditions, the plasticizer can diffuse out of the plastic [23b, 24]. Inspection of sPVC bags (sPVC implies here PVC with plasticizers) removed from long-term nuclear storage containers show signs of discoloration, unidentified liquid droplets and adhesion to the inner metal container, which also exhibit evidence of corrosion [25]. As demonstrated by numerous studies, PVC under exposure to heat and/or radiation loses hydrochloric acid (HCl) when it undergoes dehydrochlorination (DHC) [21c, 21d]. DHC of the polymer backbone induces formation of conjugated polyene sequences, discoloration of the polymer, and it can lead to appreciable off-gassing at temperatures as low as 120°C [26]. The instability of the PVC backbone and the nature of the initiation sites from which the DHC starts have been the subject of debate for many years [27]. Generally, the main proposed degradation mechanism relies on the existence of low thermal stability structural defects produced during manufacturing of the polymer, such as tertiary chloride and allylic chloride groups. A recent review by Starnes addresses this topic in greater detail [28]. Furthermore, the presence of oxygen causes a large increase in the rate of thermal DHC, along with oxidation reactions and chain scission [29]. In addition, the presence of hydroperoxides, hydroxyls, and carbonyls generated during thermal oxidative degradation are thought to participate in the DHC process. Similarly, irradiation of PVC induces formation of polyenyl radicals and DHC of the polymer backbone. In particular, LaVerne and co-workers demonstrated that Cl^- yields in the gamma radiolysis of non-plasticized PVC with number average weights of 22,000, 47,000, and 99,000 Daltons were 19.6, 33.8, and 32.5 atoms/100 eV; respectively [30]. These exceptionally large Cl^- yields suggest that a chain process involving radicals stabilized on the polymeric chain is responsible for the polymer degradation. Interestingly, those authors demonstrated that Cl^- continuously evolves from the polymer for days following exposure to ionizing radiation. Because of evolution of HCl and sPVC's limitations in terms of durability under harsh environments, we were prompted to evaluate alternative materials that would offer better resistance to aging conditions while retaining or outperforming the mechanical, chemical and thermal properties of sPVC.

Our team screened a series of polymers, including polyethylene and polyurethanes, as replacement candidates for sPVC bags. The result turned out to be that, not only polyurethanes are the most promising replacements, these also outperformed sPVC. Polyurethanes are a family of materials of great interest because of their numerous industrial applications such as adhesives, sealants, coatings, and elastomers [31]. They are composed of alternating soft segments (polyethers or polyesters) and hard polar urethane segments, formed from the reaction between a diisocyanate and one or more diols [32]. More specifically, aromatic polyether urethanes (APU-ether) and aromatic polyester urethanes (APU-ester) can be used in applications that require flexibility, strength and toughness. Our team is performing accelerated aging studies that combine thermal and gamma radiation on APU-ester and APU-ether to estimate lifetime and any corrosion issues (Figure 34). Changes in chemistry, thermal and mechanical properties due to accelerated aging are being assessed by a range of experimental techniques including infrared spectroscopy, mass spectrometry, differential scanning calorimetry, thermogravimetric analysis, nuclear magnetic resonance spectroscopy, contact angle measurements and mechanical testing. Current results from our aging study show no corrosion issues, and both APUs exhibit superior mechanical, chemical and thermal properties compared to those of sPVC (Figure 35 and Figure 36.)

Samples	Pristine	Gamma irradiated	Thermally aged	Alpha irradiated	
Aging conditions	N/A	200 kGy	10 days at 135 °C	5.24 MeV, 5×10^{13} cm^{-2}	5.24 MeV, 1×10^{14} cm^{-2}
sPVC					
APU-ether			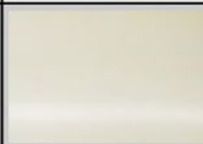		
316L coupon			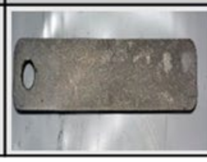	No coupon placed in the alpha exposure	No coupon placed in the alpha exposure

Figure 34. Results of accelerated aging tests performed on sPVC and APU (ether).[5, 33]

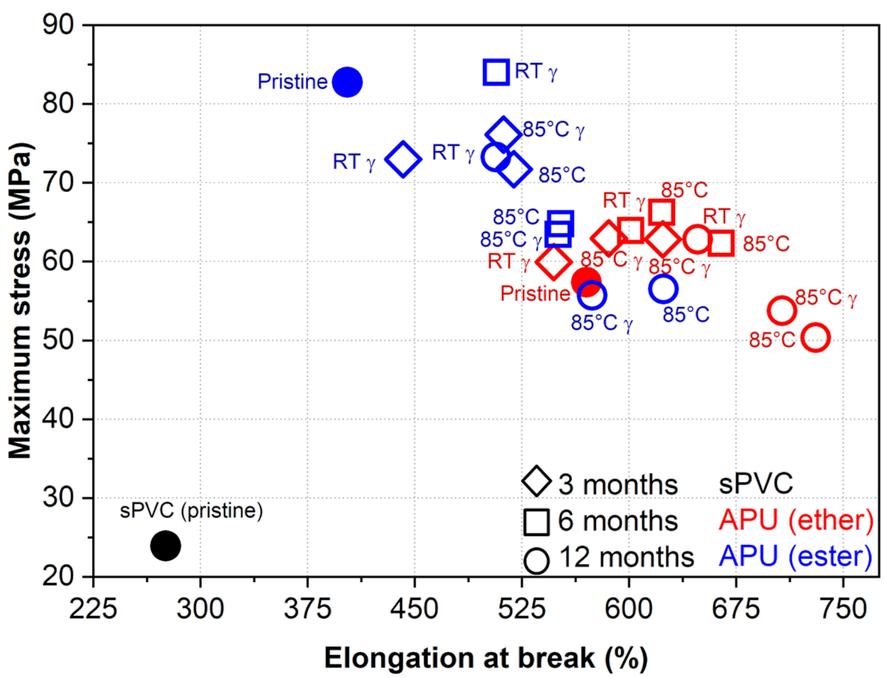

Figure 35. Results of tension testing performed on sPVC, APU (ether), and APU (ester). [5, 33]

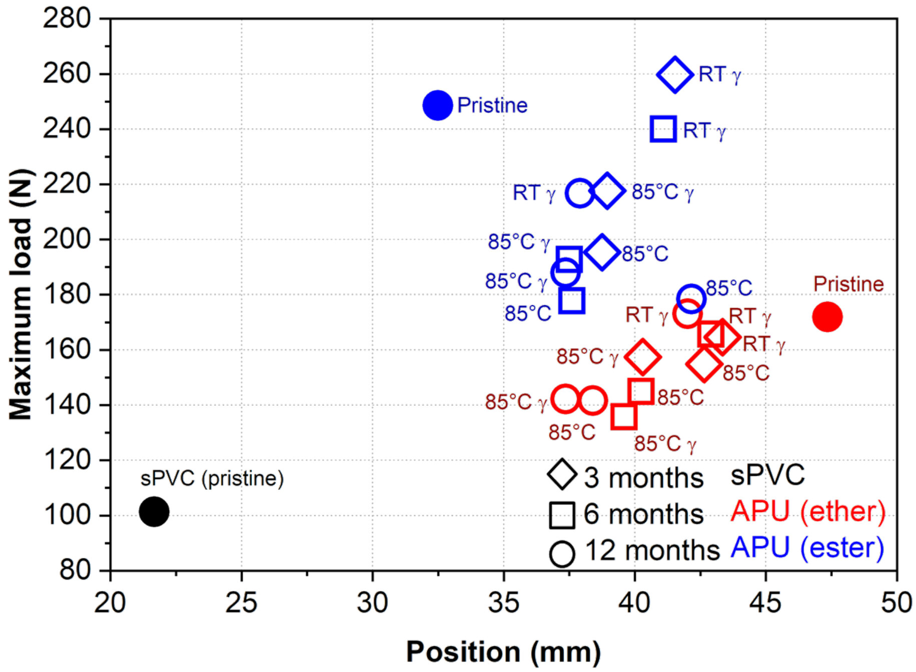

Figure 36. Results of puncture testing performed on sPVC, APU (ether), and APU (ester). [5, 33]

APU-esther and APU-ether bagout bags were tested by PF4 operators in the TA55 glovebox training laboratory[5]. The operators successfully performed an installation of both APU-ester and APU-ether bags on the bag out port and successfully tested the bags in performing a bag out. The performance of the APU bag was similar to that of PVC; however, the operators identified the need to have the bags texturized to keep the inside surface of the outer bag from adhering to the outside surface of the inner bag during the installation. LANL is currently working with NFT in the procurement of APU bag out bags for use in PF4.

6.0 Future Work

6.1 Future Surveillance

The FY19 surveillance plan targeted SAVY-4000 and Hagan containers with similar/same IDC type as containers that showed corrosion in the past as well as the previously identified "worst-case IDC groups" not yet examined.[3] Additionally, engineering judgment targeted material types that would result in higher alpha and/or gamma dose as well as a higher thermal load to the PVC bag. These materials included Pu-242 materials (MT-41 and MT-42, Pu-238 materials (MT-83) and materials high in Pu-240 (MT-56 and MT-57). These materials correspond with the containers having the heaviest deposits of corrosion in FY19 (19H1, 19H3, and 19S13) showing that engineering judgement was successful in finding challenging storage contents.

To date, 22 SAVY-4000 and Hagan containers packaged with MSE salts have had a visual inspection for corrosion in surveillance. Although targeting a particular material group has been successful in finding some of the most challenging storage contents, the results have been inconsistent. For example, the corrosion ranking for the 22 SAVY-4000 and Hagan containers packaged with MSE salts ranges from zero (no corrosion) up to three (heaviest corrosion). Additionally, surveillance of similar and identically packaged containers has shown different corrosion behavior (e.g. 19H7 and 19IoOP50) These results suggest that environmental factors such as the storage room, dose in storage, shielding or no shielding, etc. may have an impact on the corrosion behavior.

The 15-year design life for SAVY-4000 containers relies on observations from the surveillance, and the lifetime may be reassessed based on future data.[2] The surveillance program is evaluated annually and modified as necessary to adjust to observations and conclusions from annual surveillance reports and accelerated aging studies. The technical basis document for the SAVY-4000 container life extension states that, "Consideration will be given to purposely keeping some Hagan containers with corrosion challenging contents in storage as long as may be reasonable" and "consideration will be given to changing the number of annual surveillance containers in order to ensure sufficient older containers are available."

Analysis of the FY19 surveillance data is currently underway, and considerations for FY20 have not yet been made. However, the following recommendations can be made based on the observations obtained to date:

- Continue to select containers based on material types having high alpha/gamma dose as targeted by engineering judgement in FY19.
- Determine which environmental factors can be considered during container selection and incorporate available data into engineering judgement.
- Identify containers that will remain "on the shelf" for future testing and develop a long-term plan for future opening.

6.2 Laser Confocal Microscope (LCM) Analyses of Field Surveillance Items

Optical microscopy had found pitting corrosion on sections of the lids and bodies of three Hagan containers that were introduced into the glovebox line for opening (16H1, 18H7, and 19H5). Although the pit diameters can be measured with a relatively high degree of confidence, accurate measurements of the pit depths cannot be obtained.[9] As a result, the corrosion working group made a recommendation that LCM be performed on these samples similar to the one shown in Figure 37.

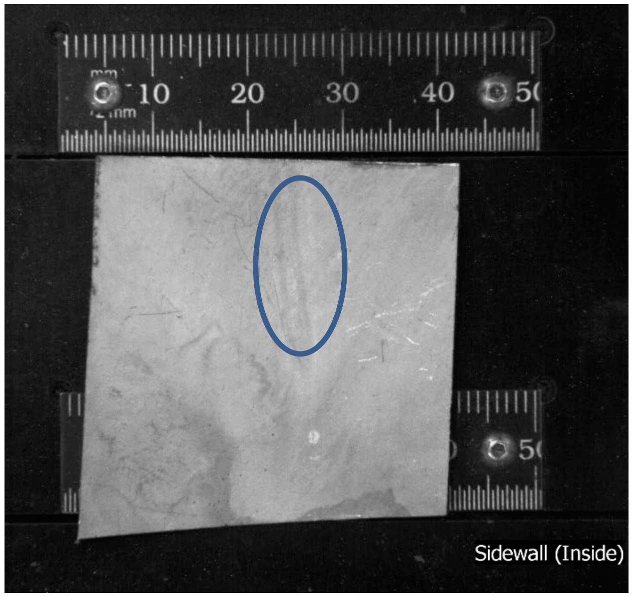

Figure 37. Sample cut from Hagan container 16H1. Pitting was located in the region where the bag was in contact with the wall (blue oval). [9]

The LCM is located in a cold laboratory at TA55. The LCM has been used to analyze contaminated stainless-steel specimens from corrosion experiments in the 3013 program.[34] The specimens are cleaned so that they are free of removable contamination, and they are loaded into a filtered, custom-designed holder like the one shown in Figure 38. A similar procedure could be performed to clean the contaminated Hagan specimens and load them in a holder. The specimens would then be removed from PF4 for LCM analysis.

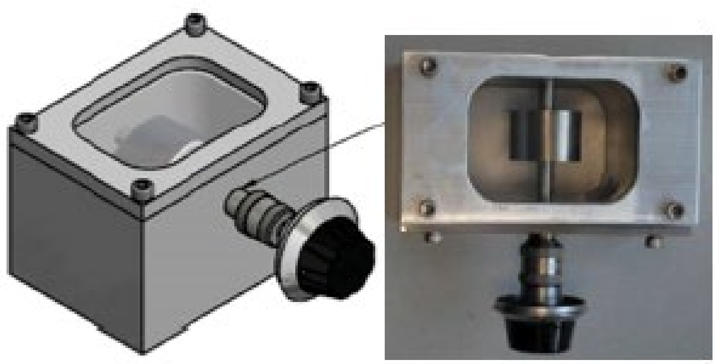

Figure 38. Holder for contaminated stainless steel specimens. [34]

The analyses would provide pit distributions and accurate measurements of pit depth. The results can be used to improve the pit growth and obtain better estimates of pit growth over time.

6.3 Automated Image Analysis

There are two forms of image analysis for corrosion on the SAVY-4000 containers, photographic images and LCM images. The idea is to use high quality image data and lower quality images to assess levels of corrosion. LCM image analysis with human inspection is resource intensive. An automated corrosion software package has been developed to reduce the time and effort needed for analysis of large numbers of LCM images. The computer program assesses general corrosion, potential pitting, and potential cracking on SAVY-4000 containers. [35] The automated image analysis can be used to quantify the pixel strength in the images; therefore, it is possible to do many types of analyses on the measurements. Depending upon the particular setup (e.g., photographic, LCM), these measurements may be of color, intensity, height or laser optical.

The SAVY's are often photographed when in surveillance and these images can be processed individually to quantify corrosion. Each individual image has a different focus quality, some are blurred and some are clear, additionally the angle and lighting can differ across images. To assess these differences, each image has to be processed individually. In an analysis of corrosion on SAVY-4000 containers, a standardized procedure was recommended to reduce the effect of camera settings on the estimated corrosion detected. [35-36]

One application of the software is to determine the amount of corrosion on an image based on the area of the features (dark spots on the images in the Figure 39) and compare areas over time. Figure 1 shows photographs of a section of a SAVY-4000 photographed in 2017 and 2018.

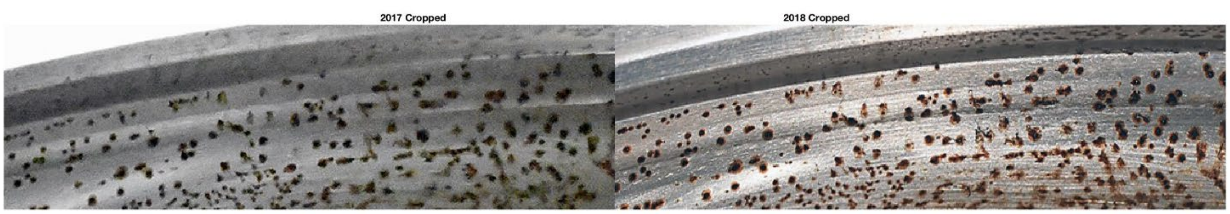

Figure 39. Photographs of the same section of a SAVY-4000 lid taken in 2017 and 2018. Comparisons of the amount of corrosion were made using the automated software.

Another application is Stringer Analysis. Stringers are small channels in the container lid, were found on the SAVY-4000 lids fabricated from a particular batch of bar stock. The image software was used to estimate the areas of the lids that had dark areas on sections, which are indicative of stringers containing MnS.[35]

Figure 40 shows a photograph of a section of a SAVY-4000 container that has stringers. The areas estimated by the software were used to estimate the quantity of MnS in the material and were compared with SAVY-4000 specifications, which have a limit on the sulfur content The software was also used to assess stringer density, as these channels could be initiation points for corrosion.

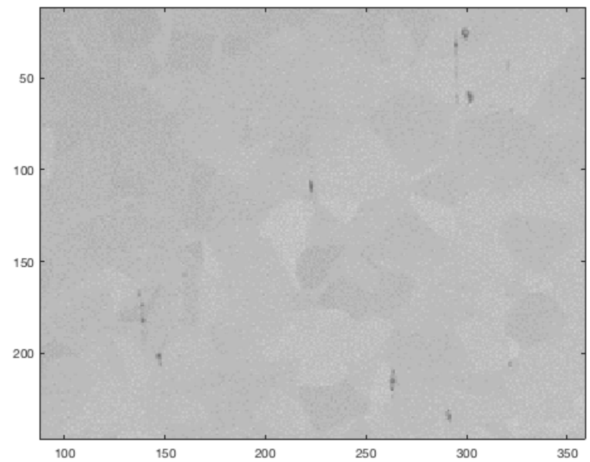

Figure 40. SAVY-4000 container photographic image with the dark areas indicative of stringers containing MnS.

The automated software can be used to identify features such as pits and cracks. LCM image analysis can be human resource intensive and detecting very small potential cracks is challenging. The automated software makes these tasks more feasible for large numbers of images. Figure 41 shows the pit depth distribution generated by the software for height data from an LCM image, with observations below 5 microns excluded. The maximum depth, average depth and the eccentricity (roundness) of the features are summarized on the figure.

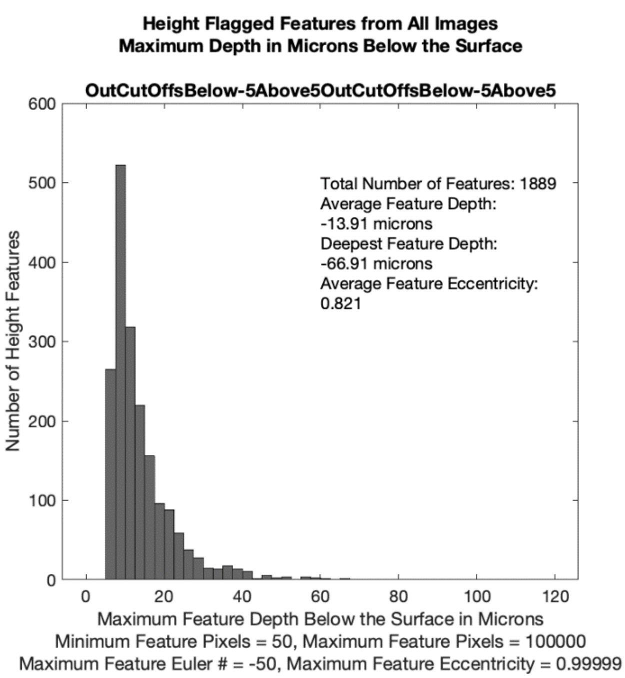

Figure 41. Pit depth distribution for a piece from a Hagan container.

The automated software can determine the location of features, such as cracks, by comparison with templates. An example of this capability is shown in Figure 42. Here, the image shows a potential crack identified in a LCM image from another container based on intensity data. The image shows several black dots, areas, which were fit to unique crack templates, and a red line, the point where a crack template was strongest. The vote strength is a metric to assess how strong the crack template match is, the higher the vote count (black dots near the template) the more likely it is a crack. The period, amplitude, and orientation, finish (proportional to the length of the crack template) are summarized on the figure.

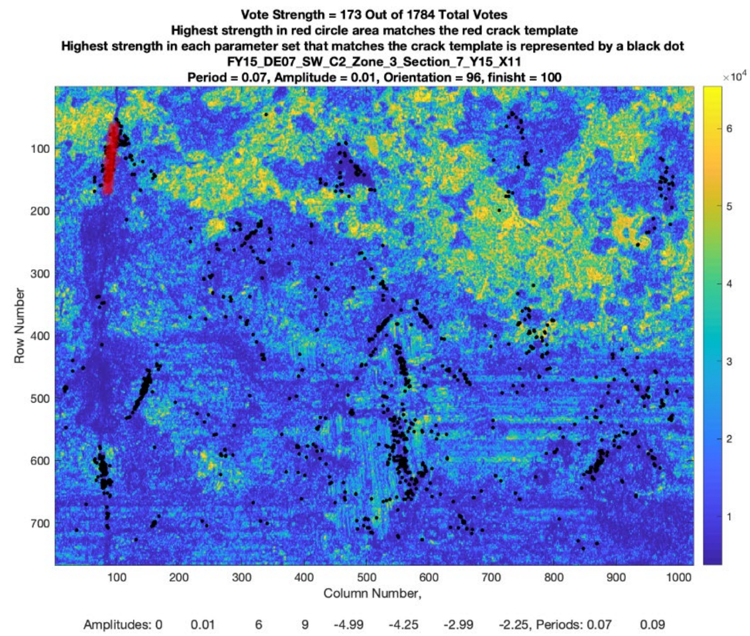

Figure 42. Identified potential crack, red line, on a piece from a 3013 container.

Using the automated software to analyze images from optical microscopy and LCM, it is possible to get more detailed information on features, pits, and cracks. The automated software can identify micron-sized cracks that can be very hard to see by visual inspection of the container or container LCM images, and can help with the processing of large numbers of images.

6.4 Nondestructive Testing

This section was contributed by Rajendra Vaidya and describes recent efforts to develop a nondestructive testing system for SAVY-4000 containers. Additional details can be found in the following report:

Vaidya, R. U.; Gigax, J. G.; Abeyta, A. A.; Davenport, M. N. *Application of Non-Destructive Testing to Assess Corrosion Damage in Nuclear Material Storage Containers*; LA-UR-19-23273; Los Alamos National Laboratory: Los Alamos, NM, 2019

The Modular Non-destructive Test System (MINTS) provides a strong technical, financial, and environmental solution for analyzing plastic deformation and corrosion of nuclear material storage containers.[37] The system combines ultrasonic (UT) and eddy current (ECA) detectors on a single platform, and its utility to test containers has been demonstrated. The use of MINTS in the surveillance program is expected to reduce the number of destructive tests necessary, thus maximizing the economic value of containers.

Efforts over the past year included the validation of the selection of UT and ECA vis-à-vis other non-destructive techniques using a detailed trade study. Results from the UT measurements completed on pristine SAVY-4000 containers have been compared to those from a Micrometer and Contour Measurement Machine (CMM). The UT results were within 2.5% of the micrometer results and 5.5% of the CMM measurements. The results are repeatable. A one tailed z-test calculated the mean difference between the values to be less than 0.0175 mm at a confidence interval of 99%. Ultrasonic testing also gives you the ability to apply a go/no-go criteria to the inspection process via signal attenuation. The minimum accurately measurable wall thickness is 0.25 mm. Below this value, the initial pulse is too close to the back-wall echo and the waveform changed dramatically rendering the measurements inaccurate. ECA is not as accurate for thickness measurements but can detect pits, cracking, and other flaws (down to 0.0762 mm).

Tests were also completed on containers extracted from the surveillance program and the wall thickness loss measured using UT was within 6% of that measured using a CMM, consistent with previous measurements.

Future work includes a double-blind experiment that will create artificial pitting and cracking in sample coupons cut out of SAVY-4000 containers. The size of these flaws will be measured by ECA and compared with a light confocal microscope (LCM). Laser Interferometry will be an integral part of the MINTS Table and will be used for external surface profiling (for residual stresses). This evaluation will be critical in looking at crack growth in the container material. Additionally, meso/microscale mechanical testing will be used to determine upper limit of external defect sizes (i.e. dents) that may lead to container failure. We will design and assemble a mechanical tester capable of performing compression/tension loading at impact strain rates (i.e. 10^3 s^{-1}) for quantitative cataloging. We will also integrate surface profiling into the system and develop software to construct 3D models of the scans as an initial condition for finite element analysis.

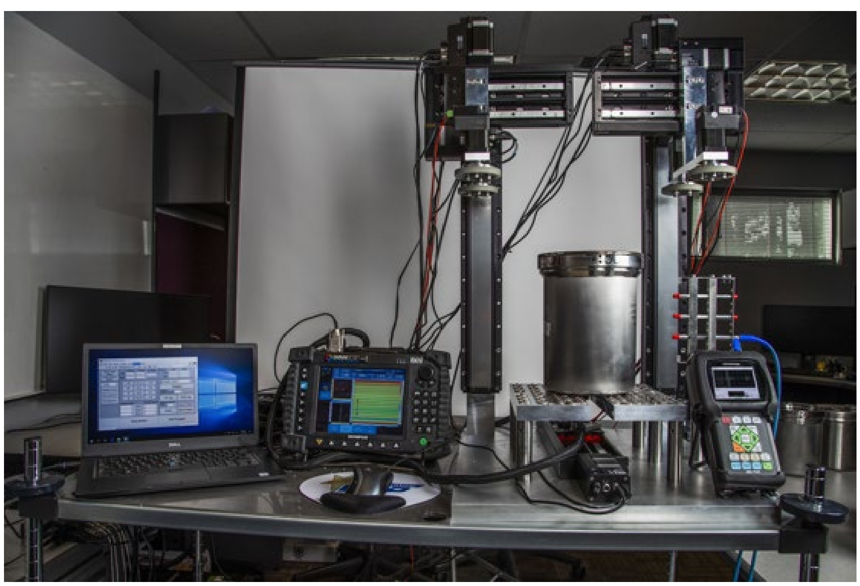

Figure 43. MINTS Table (front view).

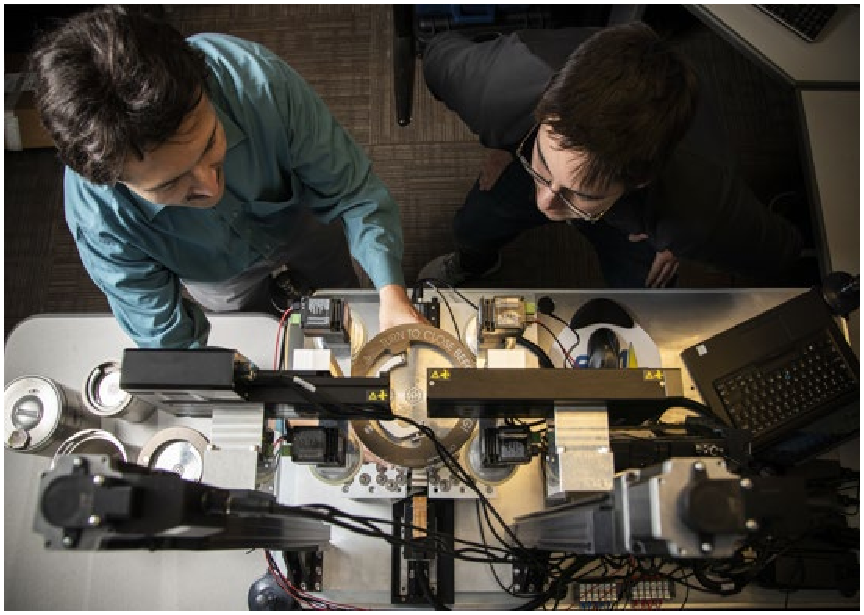

Figure 44. MINTS Table (top view).

6.5 SAI Container Cross Sectioning

Cross sectioning of dropped SAI container (081305070) is planned for FY20. Sectioning will be performed on the same areas of interest as the previous container. Pit and crack distributions as well as the aspect ratios (width/depth) will be obtained and compared those obtained for SAI container 011305020 examined previously. Comparison of the results will help to determine if the drop test has an effect on the metal defects at the microscopic (and macroscopic level). Data obtained examining the second SAI container will be used to improve the pit growth model, which is used to predict pit depth growth over time.

6.6 Accelerated Aging Studies

Analysis of SAI container 011305020 has shown that pitting and cracking can occur in SAVY-4000 containers under extreme conditions, but through-wall penetrations have not been observed. Drop testing performed on SAI container 081305070 that was exposed to the same conditions has shown that the container continues to perform its function despite the corrosion damage. Based on these results, the corrosion working group has proposed a set of experiments aimed at determining the smallest pit size (in terms of depth and circumference) that would enable a release of particles during a drop test of the SAVY-4000 and the smallest wall thickness decrement that would cause a SAVY-4000 container to release particles during the aforementioned drop. In these experiments, a SAVY-4000 container would be treated with calcium chloride solutions to produce a set of pits of varying size on the inside wall. A second SAVY-4000 would be treated with HCl to uniformly reduce the wall thickness by one-third. Pit depths would be measured by Eddy Current testing and confirmed with laser confocal microscopy. Likewise, the wall thinning would be measured by Ultrasonic Testing. The successful completion of these experiments could determine the pit size and wall thickness that would make a SAVY-4000 container release particles upon a drop scenario and would help validate Eddy Current and Ultrasonic Testing as two non-destructive techniques for *in-situ* monitoring of pitting and wall thinning in containers used for nuclear material storage. The end goal of all of these tests would establish the bounding conditions on the wall thickness and pit sizes of the SAVY-4000 containers in a corrosive environment.

6.7 PVC Replacement

An important aspect of the procurement of the new bagout bags is the composition of the polymer. If the bag material that is replacing the PVC bags is not compositionally the same it may not perform as anticipated from the testing described in Section 5.0. A test and specification is being identified to ensure that the material received by Los Alamos National Laboratory is equivalent to what has been tested. Once the acceptance tests and criteria are identified, an order will be placed for a subset of bag sizes that will be treated as a pilot to confirm that the replacement bag material satisfies the needs of the facility operators.

7.0 Conclusion

Evaluation of corrosion in SAVY-4000 and Hagan storage containers is an ongoing effort that incorporates field surveillance and laboratory studies. The greatest concern with respect to the corrosion of currently packaged SAVY-4000 and Hagan containers is through-wall cracking resulting from SCC of stainless steel. At this time, the SAVY-4000 containers have a 15-year lifetime through a 10-year extension on the 5-year design life that depends on observations from surveillance. The surveillance program and engineering judgement were successful in finding challenging contents in storage. Data also suggest that environmental factors need to be considered in container selection. General corrosion and pitting continue to be observed in surveillance containers, but cracking has not been observed. The most severe example of pitting corrosion in a storage container was found in container 16H1, which has pits of 100 to 160 microns in diameter and estimated depths of approximately 40 microns.

Accelerated aging studies performed on SAVY-4000 and Hagan containers to date have exposed both containers and specimens of both container types to a moist HCl environment. Preliminary results have found general corrosion and pitting on corrosion test specimens of both SAVY-4000 containers. Cracking was observed only in Hagan corrosion test specimens, which provides additional evidence that corrosion effects in Hagan containers are bounding of SAVY-4000 containers.

Pitting and cracking has been observed in SAI SAVY-4000 container 011305020 by LCM analysis. The conditions inside these containers are assumed as a bounding corrosive environment due to the high relative humidity and HCl vapor pressure. These conditions are similar to those used in accelerated aging studies. The maximum penetration of any of the defects was 80 microns (approximately 10% of the total wall thickness). Analysis by LCM is planned for container 081305070, which passed a helium leak test after four consecutive drops. Additional work is needed to determine the minimum size of a defect that would lead to release in a drop scenario.

8.0 References

1. U.S. Department of Energy; Office of Environment, H., Safety and Security, *Nuclear Material Packaging Manual*; DOE M 441.1-1 (Chg 1); Washington, D.C., 2016.

2. Stone, T. A.; Reeves, K. P.; Karns, T.; Smith, P. H.; Veirs, D. K. *Technical Basis Update for Design Life Extension of the SAVY-4000 Series Containers*; LA-UR-18-27269; Los Alamos National Laboratory: Los Alamos, NM, 2019.
3. Kaufeld, K. A.; Kelly, E. J.; Stone, T. A.; Smith, P. H.; Karns, T.; Prochnow, D. A.; Narlesky, J. E. *Los Alamos National Laboratory SAVY-4000 Field Surveillance Plan Update for 2019*; LA-UR-19-24424; Los Alamos National Laboratory: Los Alamos, NM, 2019.
4. Smith, P. H.; Yarbro, T. F.; Veirs, D. K.; Prochnow, D. A.; Brabec, C. L. *Using Container Survey Data to Assign Risk to Nuclear Material Packages*; LA-UR-17-24589; Los Alamos National Laboratory: Los Alamos, NM, 2017.
5. Dumont, J. H.; Crum, S. L. A.; Zhao, C.; Murphy, E. C.; Reardon, S. D.; Lee, S. Y.; Lee, K.-S.; Labouriau, A.; Karns, T.; Smith, P. H. *Functional Testing of Alternative Bag-Out Bag for PF-4 Implementation*; LA-UR-18-25708; Los Alamos National Laboratory: Los Alamos, NM, 2018.
6. (a) Rios, D.; Gaunt, A. J.; Narlesky, J. E.; Berg, J. M.; Veirs, D. K.; Worl, L. A. *Capture, Identification and Quantification of the Elusive Chlorine-Containing Gases Emitted from Hydrated PuO2/Salt Mixtures*; LA-UR-17-27871; Los Alamos National Laboratory: Los Alamos, NM, 2017; (b) LaVerne, J. A.; Tandon, L., H_2 and Cl_2 production in the radiolysis of calcium and magnesium chlorides and hydroxides. *Journal of Physical Chemistry A* **2005,** *109* (12), 2861-2865.
7. Rios, D.; Gaunt, A. J.; Narlesky, J. E. *Generation of HCl Gas from Molten Salt Extraction Residue (XBPS333)*; LA-UR-17-28276; Los Alamos National Laboratory: Los Alamos, NM, 2017.
8. Reeves, K. P.; Karns, T.; Stone, T. A.; Narlesky, J. E.; Hyer, H. C.; Smith, P. H.; Wilson, K. V.; Duque, J.; Stroud, M. A.; Berg, J. M.; Gaunt, A. J.; Rios, D. *Evaluating Corrosion Effects on the Stainless Steel Components of the SAVY-4000/Hagan Nuclear Material Storage Containers*; LA-UR-18-25709; Los Alamos National Laboratory: Los Alamos, NM, 2018.
9. Narlesky, J. E.; Wilson, K. V.; Kelly, E. J. *Microscopic Examination of the Corroded Hagan Container Used to Store Molten Salt Extraction Residue XBPS333*; LA-UR-17-28355; Los Alamos National Laboratory: Los Alamos, NM, 2018.
10. In *Standard Practice for Evaluating Stress-Corrosion-Cracking Resistance of Metals and Alloys in a Boiling Magnesium Chloride Solution*, ASTM International: West Conshohocken, PA, 2018.
11. In *Standard Test Method for Determining Residual Stresses by the Hole-Drilling Strain-Gage Method*, ASTM International: West Conshohocken, PA, 2013.
12. Karns, T.; Oka, J. M.; Reeves, K. P.; Kaufeld, K. A.; Smith, P. H.; Stone, T. A.; Narlesky, J. E.; Kelly, E. J. *Surveillance Report on SAVY 4000 and Hagan Nuclear Material Storage Containers for Fiscal Year 2018*; LA-UR-18-31604; Los Alamos National Laboratory: Los Alamos, NM, 2018.
13. Reeves, K. P.; Weis, E.; Blair, M. W.; Moore, M. E.; Karns, T.; Oka, J. M.; Herman, M. J.; Prochnow, D. A.; Smith, P. H.; Stone, T. A.; Veirs, D. K.; Narlesky, J. E. *LANL Storage Container Surveillance Report*; LA-UR-16-27427; Los Alamos National Laboratory: Los Alamos, NM, 2016.
14. Fritz, J. J.; Fuget, C. R., Vapor Pressure of Aqueous Hydrogen Chloride Solutions 0 ºC to 50 ºC. *Industrial and Engineering Chemistry* **1956,** *1* (1).
15. Narlesky, J. E.; Aragon, S. M.; Colletti, L. M.; Garduno, K.; Klundt, D. J.; Lower, G. L. M.; Martinez, P. T.; Mathew, K. J.; Schwartz, D. S.; Slemmons, A. K.; Willson, S. P.; Xu, N. *Chemical Analysis of the White and Brown Coatings Found on Corroded Hagan and SAVY 4000 Containers*; LA-UR-17-28753; Los Alamos National Laboratory: Los Alamos, NM, 2017.

16. Reeves, K. P.; Karns, T.; Weis, E.; Oka, J. M.; Smith, P. H.; Stone, T. A.; Narlesky, J. E. *Surveillance Report on SAVY-4000 and Hagan Nuclear Material Storage Containers for FY 2017*; LA-UR-17-31263; Los Alamos National Laboratory: Los Alamos, NM, 2017.
17. Duque, J. G.; Hill, M. A.; Bohn, K.; Reeves, K. P.; Karns, T.; Rios, D.; Wendelberger, J. G.; Lopez, L.; Narlesky, J. E.; Kelly, E. J.; Kaufeld, K. A.; Vaidya, R.; Oka, J. M.; Stone, T. A.; Smith, P. H. *Microscopic Characterization of Corrosion of SAVY-4000: SAI Container*; LA-UR-19-28733; Los Alamos National Laboratory: Los Alamos, NM, 2019.
18. Duque, J.; Veirs, D. K.; Hill, M. A.; Berg, J. M.; Worl, L. A.; Kelly, E. J.; Narlesky, J. E.; Lillard, R. S.; Harradine, D. M. *Corrosion of Teardrop Specimens Exposed to Cerium Oxide-Chloride Salt Mixtures*; LA-UR-12-26881; Los Alamos National Laboratory: Los Alamos, NM, 2012.
19. Rios, D.; Duque, J.; Wendelberger, J. G. *Accelerated Corrosion Studies with SAVY-4000 and Hagan Containers*; LA-UR-19-28711; Los Alamos National Laboratory: Los Alamos, NM, 2019.
20. Rios, D.; Berg, J. M.; Duque, J.; Tung, D. C.; Veirs, D. K.; Worl, L. A. *Corrosion of 304L SS Teardrops Exposed to Chlorine-Containing Gases in Aerobic and Anaerobic Environments*; LA-UR-17-28850; Los Alamos National Laboratory: Los Alamos, NM, 2017.
21. (a) Titow, M., *PVC technology*. Springer Science & Business Media: 2012; (b) Babinsky, R., PVC additives: a global review. *Plastics, Additives and Compounding* **2006,** *8* (1), 38-40; (c) Zweifel, H.; Maier, R.; Schiller, M., *Plastics Additives Handbook 6E*. Hanser, München: 2009; (d) Yu, J.; Sun, L.; Ma, C.; Qiao, Y.; Yao, H., Thermal degradation of PVC: A review. *Waste management* **2016,** *48*, 300-314.
22. Daniels, P. H., A brief overview of theories of PVC plasticization and methods used to evaluate PVC-plasticizer interaction. *Journal of vinyl and additive technology* **2009,** *15* (4), 219-223.
23. (a) Mauritz, K. A.; Storey, R. F.; George, S. E., A general free volume-based theory for the diffusion of large molecules in amorphous polymers above the glass temperature. I. Application to di-n-alkyl phthalates in PVC. *Macromolecules* **1990,** *23* (2), 441-450; (b) Afshari, A.; Gunnarsen, L.; Clausen, P.; Hansen, V., Emission of phthalates from PVC and other materials. *Indoor Air* **2004,** *14* (2), 120-128.
24. Graham, P., Phthalate ester plasticizers--why and how they are used. *Environmental health perspectives* **1973,** *3*, 3.
25. Reeves, K. P.; Karns, T.; Stone, T. A.; Narlesky, J. E.; Hyer, H. C.; Smith, P. H.; Wilson Jr, K. V.; Duque, J.; Stroud, M. A.; Berg, J. M. *Evaluating Corrosion Effects on the Stainless Steel Components of the SAVY-4000/Hagan Nuclear Material Storage Containers*; Los Alamos National Lab.(LANL), Los Alamos, NM (United States): 2018.
26. Krzymien, M. E. In *PVC photo-oxidative degradation: Identification of volatiles*, Macromolecular Symposia, Wiley Online Library: 1997; pp 27-40.
27. (a) Winkler, D., Mechanism of polyvinyl chloride degradation and stabilization. *Journal of Polymer Science* **1959,** *35* (128), 3-16; (b) Baum, B.; Wartman, L., Structure and mechanism of dehydrochlorination of polyvinyl chloride. *Journal of Polymer Science* **1958,** *28* (118), 537-546.
28. Starnes Jr, W., Overview and assessment of recent research on the structural defects in poly (vinyl chloride). *Polymer degradation and stability* **2012,** *97* (9), 1815-1821.
29. Talamini, G.; Pezzin, G., Kinetic Study on the Reaction of Polyvinyl Chloride Thermal Dehydrochlorination. *Makromolekul Chem* **1960,** *39* (1), 26-38.
30. LaVerne, J. A.; Carrasco-Flores, E. A.; Araos, M. S.; Pimblott, S. M., Gas production in the radiolysis of poly(vinyl chloride). *J Phys Chem A* **2008,** *112* (15), 3345-3351.

31. (a) Engels, H. W.; Pirkl, H. G.; Albers, R.; Albach, R. W.; Krause, J.; Hoffmann, A.; Casselmann, H.; Dormish, J., Polyurethanes: versatile materials and sustainable problem solvers for today's challenges. *Angewandte Chemie International Edition* **2013,** *52* (36), 9422-9441; (b) Wirpsza, Z., *Polyurethanes: chemistry, technology, and applications*. Ellis Horwood: 1993; (c) Szycher, M., *Szycher's handbook of polyurethanes*. CRC press: 1999.
32. (a) Król, P., Synthesis methods, chemical structures and phase structures of linear polyurethanes. Properties and applications of linear polyurethanes in polyurethane elastomers, copolymers and ionomers. *Progress in Materials Science* **2007,** *52* (6), 915-1015; (b) Hepburn, C., *Polyurethane elastomers*. Springer Science & Business Media: 2012.
33. (a) Dumont, J. H.; al., e., Aging of Aromatic Polyurethanes Bags for Nuclear Storage. *Transactions of the American Nuclear Society* **2019,** *120*, 417-418; (b) Dumont, J. H.; al., e., Effects of thermal aging and ionizing radiation on sPVC and aromatic polyether urethane used to store nuclear materials. *Polymer Testing* **2019,** *78*.
34. Duque, J.; Stroud, M. A.; Narlesky, J. E.; Rios, D.; Kelly, E. J.; Joyce, S. A.; Berg, J. M.; Veirs, D. K.; Worl, L. A. *Microscopic Characterization of Corrosion of Teardrop Specimens Exposed to Plutonium-Bearing Materials with Calcium Chloride Impurities*; LA-UR-19-28748; Los Alamos National Laboratory: Los Alamos, NM, 2019.
35. Wendelberger, J. G. *Data Visualization for Statistical Analysis and Discovery in Container Surface Characterization at the Nano-Scale and Micro-Scale*; LA-UR-18-28049; Los Alamos National Laboratory: Los Alamos, NM, 2018.
36. Duque, J.; Wendelberger, J. G.; Rios, D. *Accelerated Corrosion Experiments with SAVY and Hagan Containers*; LA-UR-19-24808; Los Alamos National Laboratory: Los Alamos, NM, 2019.
37. Vaidya, R. U.; Gigax, J. G.; Abeyta, A. A.; Davenport, M. N. *Application of Non-Destructive Testing to Assess Corrosion Damage in Nuclear Material Storage Containers*; LA-UR-19-23273; Los Alamos National Laboratory: Los Alamos, NM, 2019.